Today's outline - March 31, 2020 (part A)

Today's outline - March 31, 2020 (part A)

- In situ studies of methanol fuel cells

Today's outline - March 31, 2020 (part A)

- In situ studies of methanol fuel cells
    1. Pt/Ni cathode catalyst

Today's outline - March 31, 2020 (part A)

- In situ studies of methanol fuel cells
    1. Pt/Ni cathode catalyst
    2. Role of Ru in methanol oxidation

Today's outline - March 31, 2020 (part A)

- In situ studies of methanol fuel cells
  1. Pt/Ni cathode catalyst
  2. Role of Ru in methanol oxidation

Homework Assignment #05:
Chapter 5: 1, 3, 7, 9, 10
due Thursday, April 02, 2020

Today's outline - March 31, 2020 (part A)

- In situ studies of methanol fuel cells
    1. Pt/Ni cathode catalyst
    2. Role of Ru in methanol oxidation

Homework Assignment #05:
Chapter 5: 1, 3, 7, 9, 10
due Thursday, April 02, 2020

Homework Assignment #06:
Chapter 6: 1,6,7,8,9
due Tuesday, April 14, 2020

Mark I operando fuel cell

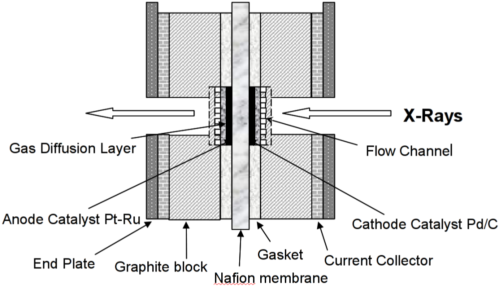

- Transmission mode
- <1 mm of graphite
- Pt/Ru on anode
- Pd on cathode
- 35°C operating temp
- 1-2 min scan time

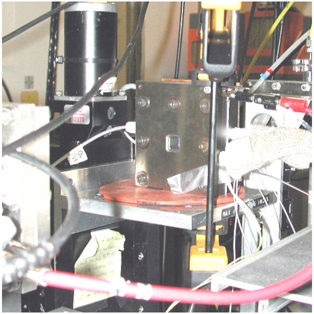

R. Viswanathan et al., "In-situ XANES study of carbon supported Pt-Ru anode electrocatalysts for reformate-air polymer electrolyte fuel cells", *J. Phys. Chem.* **B 106**, 3458 (2002).

Mark II operando fuel cell

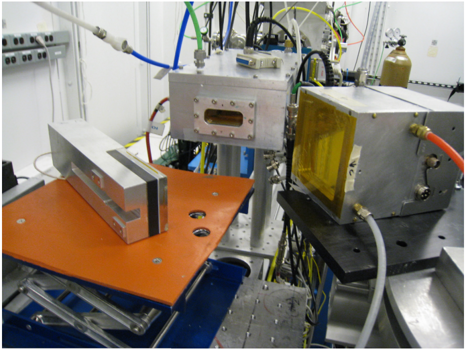

- Air-breathing cathode
- Pd on anode
- $1.2\,\mathrm{mg/cm^2}$ loading
- $50^\circ\mathrm{C}$ operating temp
- Pt L_3 and Ni K edges
- Continuous scan mode @

mrcat

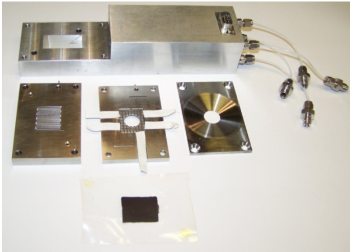

E.A. Lewis et al., "Operando x-ray absorption and infrared fuel cell spectroscopy", *Electrochim. Acta.* **56**, 8827 (2011).

Oxygen reduction at a PtNi cathode

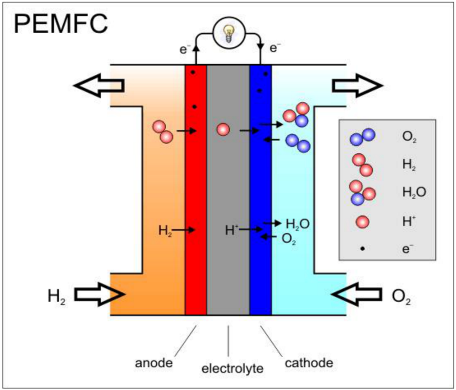

U.S. Department of Defense (DoD) Fuel Cell Test and Evaluation Center (FCTec)

Anode: 0 V vs. SHE

$$2\,H_2 \longrightarrow 4\,H^+ + 4\,e^-$$

Oxygen reduction at a PtNi cathode

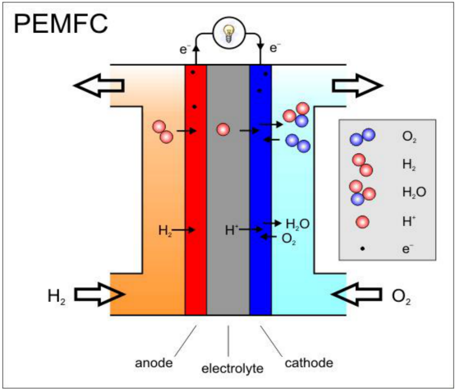

U.S. Department of Defense (DoD) Fuel Cell Test and Evaluation Center (FCTec)

Anode: 0 V vs. SHE

$$2\,H_2 \longrightarrow 4\,H^+ + 4\,e^-$$

Cathode: 1.23 V vs. SHE

$$O_2 + 4\,H^+ + 4\,e^- \longrightarrow 2\,H_2O$$

Oxygen reduction at a PtNi cathode

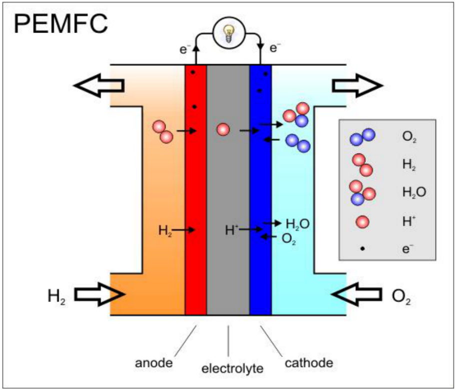

U.S. Department of Defense (DoD) Fuel Cell Test and Evaluation Center (FCTec)

Anode: 0 V vs. SHE

$$2\,H_2 \longrightarrow 4\,H^+ + 4\,e^-$$

Cathode: 1.23 V vs. SHE

$$O_2 + 4\,H^+ + 4\,e^- \longrightarrow 2\,H_2O$$

Oxygen reduction at a PtNi cathode

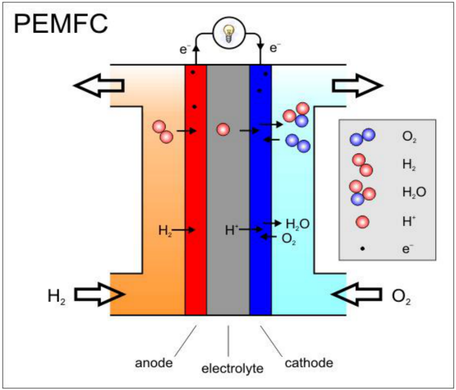

U.S. Department of Defense (DoD) Fuel Cell Test and Evaluation Center (FCTec)

Anode: 0 V vs. SHE

$$2\,H_2 \longrightarrow 4\,H^+ + 4\,e^-$$

Cathode: 1.23 V vs. SHE

$$O_2 + 4\,H^+ + 4\,e^- \longrightarrow 2\,H_2O$$

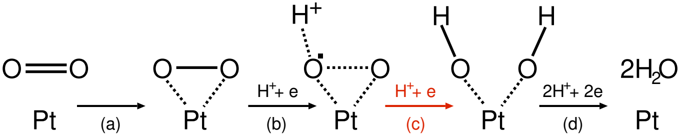

Oxygen reduction at a PtNi cathode

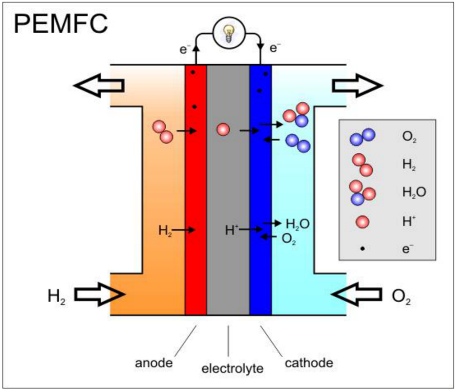

U.S. Department of Defense (DoD) Fuel Cell Test and Evaluation Center (FCTec)

Anode: 0 V vs. SHE

$$2\,H_2 \longrightarrow 4\,H^+ + 4\,e^-$$

Cathode: 1.23 V vs. SHE

$$O_2 + 4\,H^+ + 4\,e^- \longrightarrow 2\,H_2O$$

breaking O—O bond is the rate limiting step

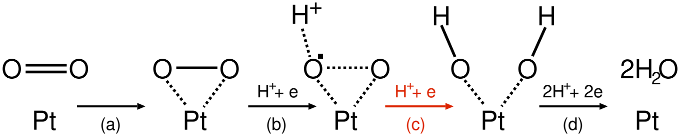

Fuel cell performance and open questions

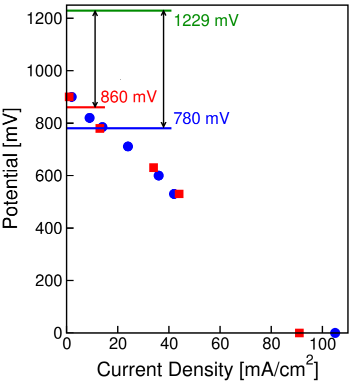

PtNi/Pd has higher open circuit voltage, similar performance to Pt/Pd.

Fuel cell performance and open questions

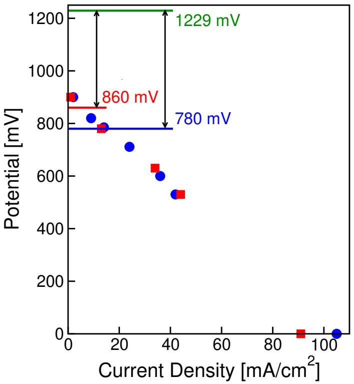

PtNi/Pd has higher open circuit voltage, similar performance to Pt/Pd.

Why is ORR improved with bimetallic catalyst?

Fuel cell performance and open questions

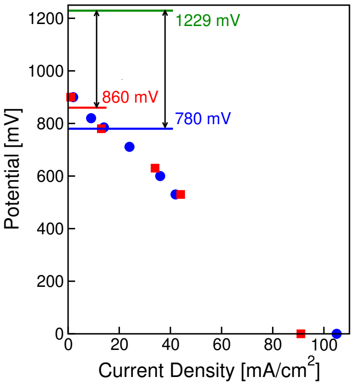

PtNi/Pd has higher open circuit voltage, similar performance to Pt/Pd.

Why is ORR improved with bimetallic catalyst?

- Pt electronic structure modified

Fuel cell performance and open questions

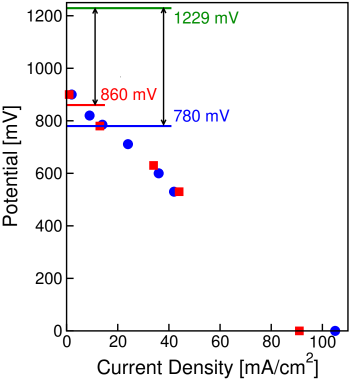

PtNi/Pd has higher open circuit voltage, similar performance to Pt/Pd.

Why is ORR improved with bimetallic catalyst?

- Pt electronic structure modified
- Pt catalyst geometric structure modified

Fuel cell performance and open questions

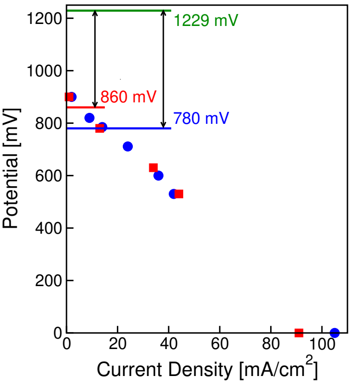

PtNi/Pd has higher open circuit voltage, similar performance to Pt/Pd.

Why is ORR improved with bimetallic catalyst?

- Pt electronic structure modified
- Pt catalyst geometric structure modified
- Static oxygen adsorbates inhibited

Fuel cell performance and open questions

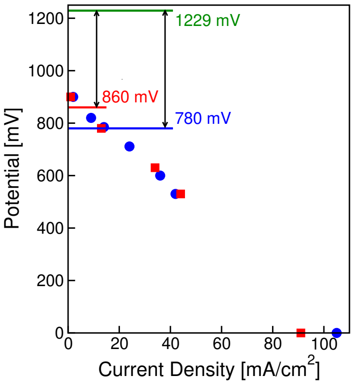

PtNi/Pd has higher open circuit voltage, similar performance to Pt/Pd.

Why is ORR improved with bimetallic catalyst?

- Pt electronic structure modified
- Pt catalyst geometric structure modified
- Static oxygen adsorbates inhibited
- Overpotential reduced

Fuel cell performance and open questions

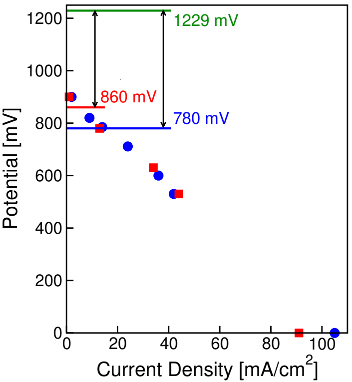

PtNi/Pd has higher open circuit voltage, similar performance to Pt/Pd.

Why is ORR improved with bimetallic catalyst?

- Pt electronic structure modified
- Pt catalyst geometric structure modified
- Static oxygen adsorbates inhibited
- Overpotential reduced

Using XAS to study the catalyst nanoparticles can help answer the first three questions

Pt/C and PtNi/C comparison

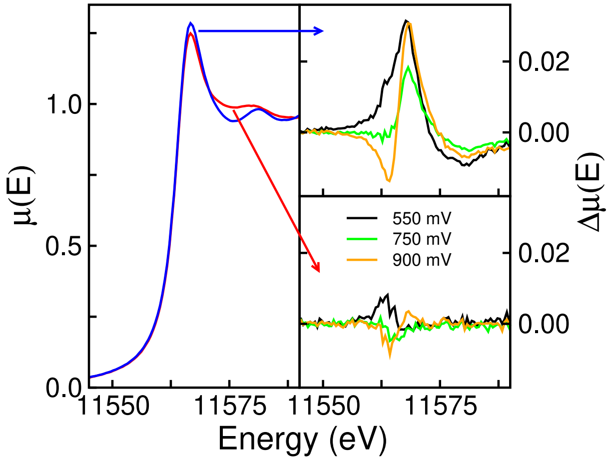

Q. Jia et al, "In Situ XAFS studies of the oxygen reduction reaction on carbon supported Pt and PtNi(1:1) catalysts", *J. Phys. Conf. Series* **190**, 012157 (2009).

Pt/C and PtNi/C comparison

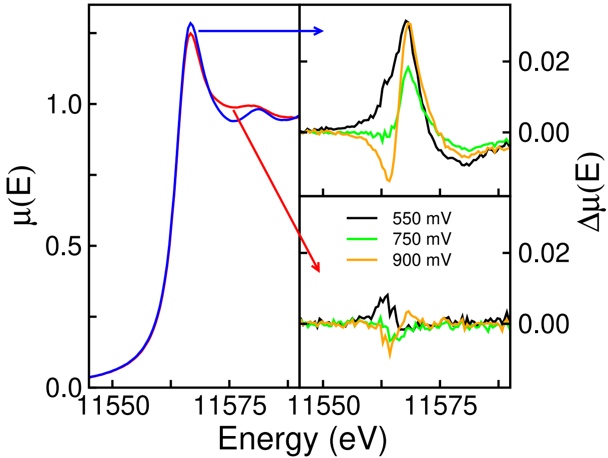

At highest potential, all catalysts are metallic and the Pt L_3 XANES shows significant difference between the Pt and PtNi catalysts

Q. Jia et al, "In Situ XAFS studies of the oxygen reduction reaction on carbon supported Pt and PtNi(1:1) catalysts", *J. Phys. Conf. Series* **190**, 012157 (2009).

Pt/C and PtNi/C comparison

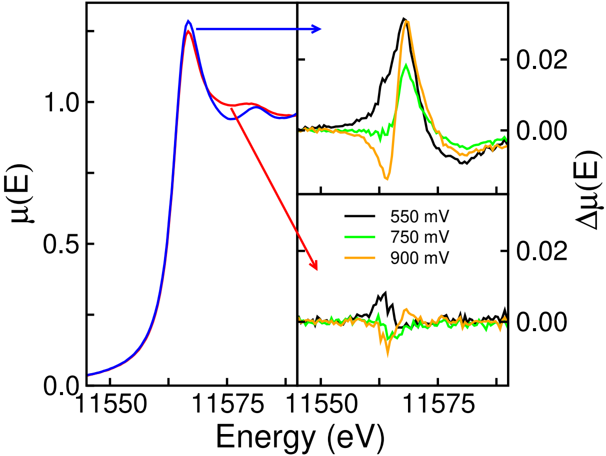

At highest potential, all catalysts are metallic and the Pt L_3 XANES shows significant difference between the Pt and PtNi catalysts

Delta XANES shows a supression of Pt oxidation in the PtNi catalyst as a function of applied potential

Q. Jia et al, "In Situ XAFS studies of the oxygen reduction reaction on carbon supported Pt and PtNi(1:1) catalysts", *J. Phys. Conf. Series* **190**, 012157 (2009).

PtNi structural model

Attempt to get global information about the oxygen

PtNi structural model

Attempt to get global information about the oxygen

Fit all potentials with same metal core parameters for each catalyst

PtNi structural model

Attempt to get global information about the oxygen

Fit all potentials with same metal core parameters for each catalyst

Simultaneous fit of Pt and Ni edges in PtNi/C with constraint on Pt-Ni distance

PtNi structural model

Attempt to get global information about the oxygen

Fit all potentials with same metal core parameters for each catalyst

Simultaneous fit of Pt and Ni edges in PtNi/C with constraint on Pt-Ni distance

Fit in k, k^2, and k^3 weighting simultaneously

PtNi structural model

Attempt to get global information about the oxygen

Fit all potentials with same metal core parameters for each catalyst

Simultaneous fit of Pt and Ni edges in PtNi/C with constraint on Pt-Ni distance

Fit in k, k^2, and k^3 weighting simultaneously

Apply M-O path constraints

- length common across potentials
- σ^2 fixed to 0.01
- Pt-O in PtNi/C at all potentials are refined with a common occupation #

Example fits

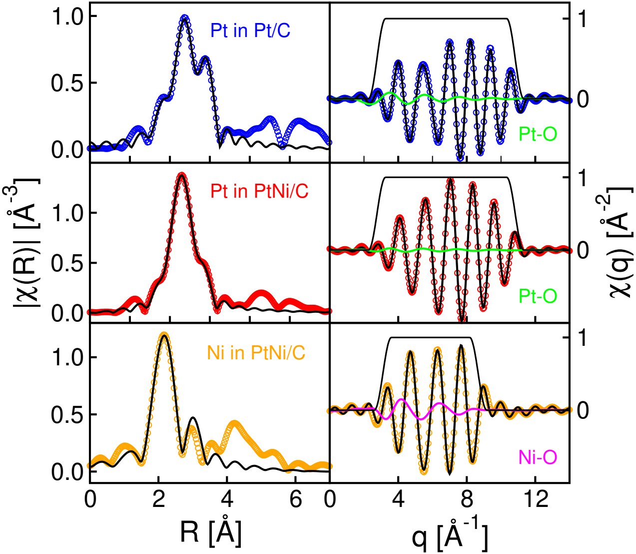

"In Situ XAFS studies of the oxygen reduction reaction on carbon supported Pt and PtNi(1:1) catalysts", Q. Jia, E.A. Lewis, E.S. Smotkin, and C.U. Segre, *J. Phys. Conf. Series* **190**, 012157 (2009).

Example fits

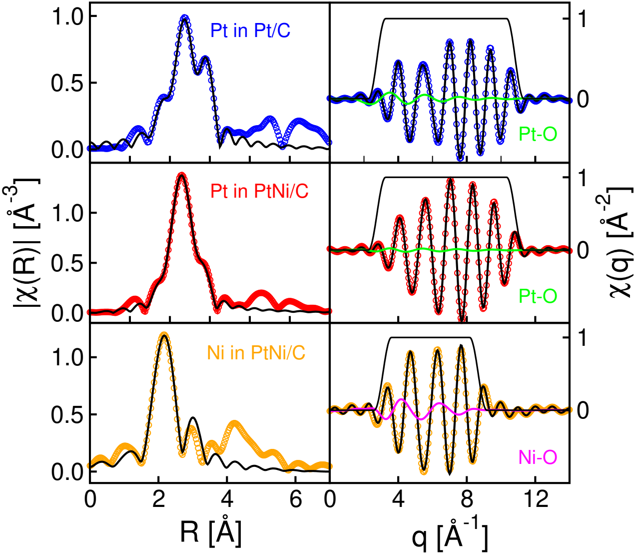

Fits out to 3.5 Å in R-space and back Fourier Transforms

"In Situ XAFS studies of the oxygen reduction reaction on carbon supported Pt and PtNi(1:1) catalysts", Q. Jia, E.A. Lewis, E.S. Smotkin, and C.U. Segre, *J. Phys. Conf. Series* **190**, 012157 (2009).

Example fits

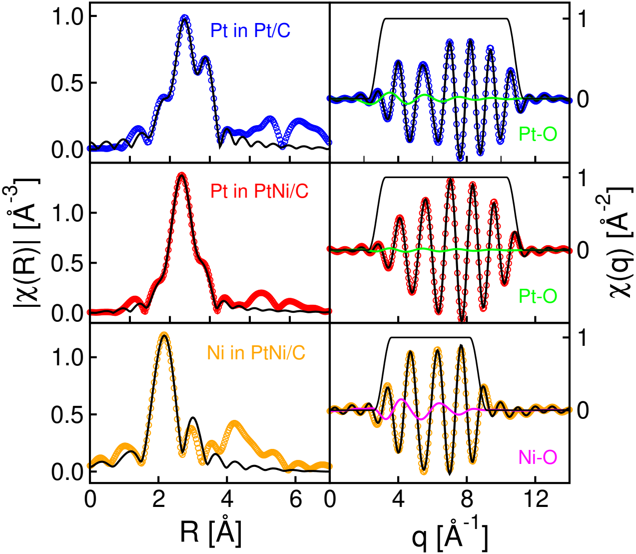

Fits out to 3.5 Å in R-space and back Fourier Transforms

The Pt catalyst shows a larger oxygen path contribution than the PtNi catalyst

"In Situ XAFS studies of the oxygen reduction reaction on carbon supported Pt and PtNi(1:1) catalysts", Q. Jia, E.A. Lewis, E.S. Smotkin, and C.U. Segre, *J. Phys. Conf. Series* **190**, 012157 (2009).

Example fits

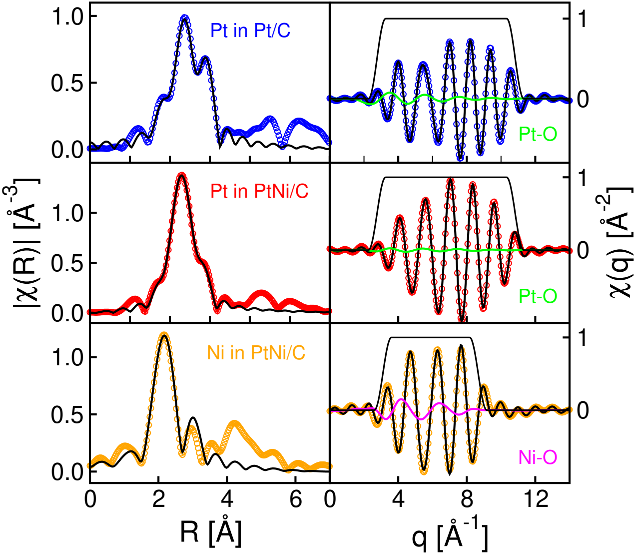

Fits out to 3.5 Å in R-space and back Fourier Transforms

The Pt catalyst shows a larger oxygen path contribution than the PtNi catalyst

The Ni EXAFS is dominated by the presence of a significant Ni-O bond

"In Situ XAFS studies of the oxygen reduction reaction on carbon supported Pt and PtNi(1:1) catalysts", Q. Jia, E.A. Lewis, E.S. Smotkin, and C.U. Segre, *J. Phys. Conf. Series* **190**, 012157 (2009).

Fit results

Pt/C		PtNi/C			
		Pt		Ni	
N_{Pt}	8.7 ± 0.2	N_{Pt}	6.1 ± 0.3	N_{Ni}	3.7 ± 0.2
$R_{\text{Pt-Pt}}$	2.749 ± 0.001	$R_{\text{Pt-Pt}}$	2.692 ± 0.003	$R_{\text{Ni-Ni}}$	2.572 ± 0.006
		N_{Ni}	3.4 ± 0.1	N_{Pt}	8.9 ± 0.5
		$R_{\text{Pt-Ni}}$	2.635 ± 0.004		
		N_{Total}	9.5 ± 0.4	N_{Total}	12.6 ± 0.7
$R_{\text{Pt-O}}$	2.02 ± 0.01	$R_{\text{Pt-O}}$	2.09 ± 0.03	$R_{\text{Ni-O}}$	1.90 ± 0.01

Note the Pt-Pt and Pt-O bond lengths as well as total metal near neighbors

"In Situ XAFS studies of the oxygen reduction reaction on carbon supported Pt and PtNi(1:1) catalysts", Q. Jia, E.A. Lewis, E.S. Smotkin, and C.U. Segre, *J. Phys. Conf. Series* **190**, 012157 (2009).

Role of Ru in CO oxidation?

- PtRu bifunctional catalyst improves performance
- In commercial PtRu catalysts there is always a lot of inactive Ru-oxide (?)
- Ru signal dominated by metallic Ru environment
- How does Ru behave in the presence of reactants adsorbed on platinum surface?

Core-shell nanoparticles can resolve these questions

Ru-decorated Pt nanoparticles

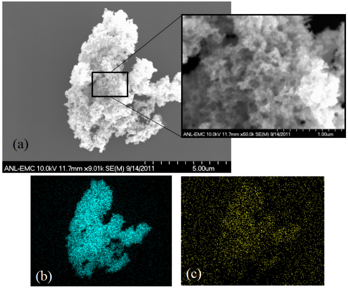

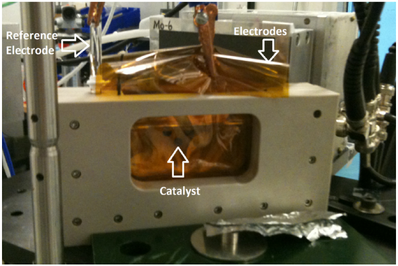

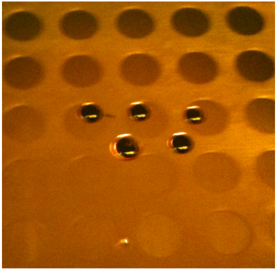

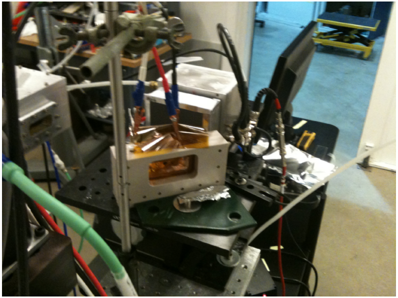

Electrochemical performance

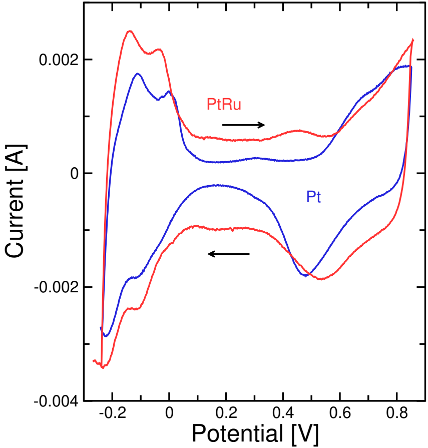

Without Methanol

Low V peaks are H^+ stripping

Dip at ∼0.5 V is oxygen stripping

Ru shifts potential on all peaks

"In situ Ru K-Edge x-ray absorption spectroscopy study of methanol oxidation mechanisms on model submonolayer Ru on Pt nanoparticle electrocatalyst," C.J. Pelliccione, E.V. Timofeeva, J.P. Katsoudas, and C.U. Segre, *J. Phys. Chem.* **C 117**, 18904 (2013).

Electrochemical performance

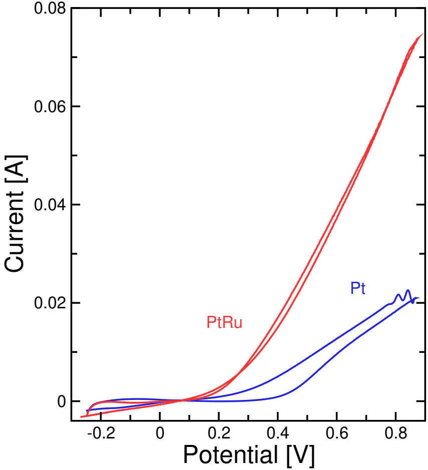

Without Methanol

Low V peaks are H^+ stripping

Dip at ∼0.5 V is oxygen stripping

Ru shifts potential on all peaks

With Methanol

Continual current growth is due to methanol oxidation

Ru improves current by removing the CO which blocks active sites

"In situ Ru K-Edge x-ray absorption spectroscopy study of methanol oxidation mechanisms on model submonolayer Ru on Pt nanoparticle electrocatalyst," C.J. Pelliccione, E.V. Timofeeva, J.P. Katsoudas, and C.U. Segre, *J. Phys. Chem.* **C 117**, 18904 (2013).

Ru EXAFS

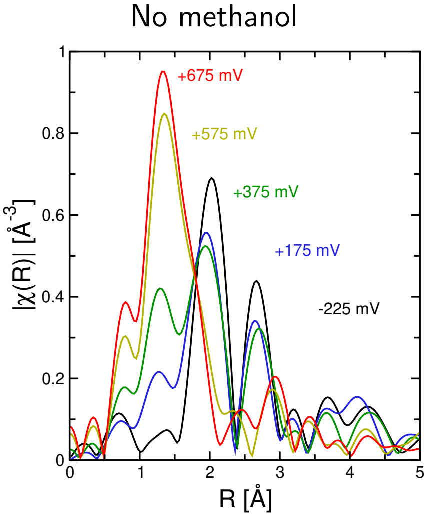

"In situ Ru K-Edge x-ray absorption spectroscopy study of methanol oxidation mechanisms on model submonolayer Ru on Pt nanoparticle electrocatalyst," C.J. Pelliccione, E.V. Timofeeva, J.P. Katsoudas, and C.U. Segre, *J. Phys. Chem.* **C 117**, 18904 (2013).

Ru EXAFS

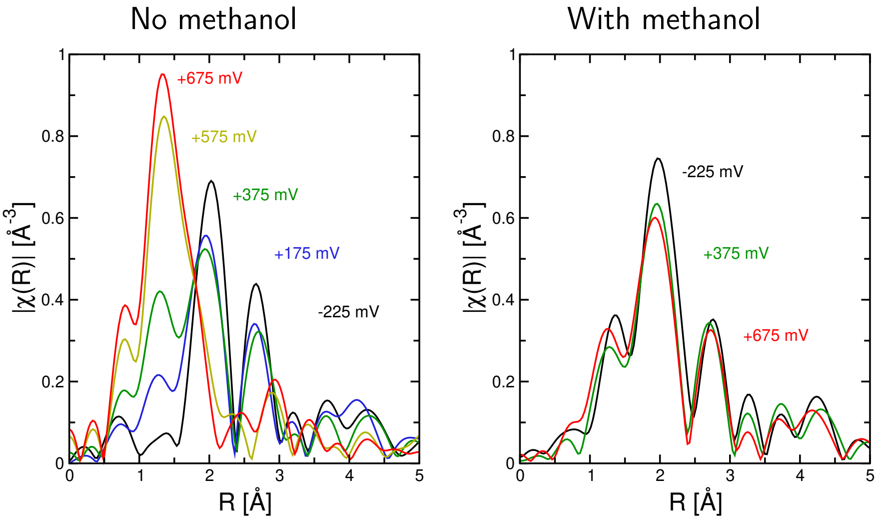

"In situ Ru K-Edge x-ray absorption spectroscopy study of methanol oxidation mechanisms on model submonolayer Ru on Pt nanoparticle electrocatalyst," C.J. Pelliccione, E.V. Timofeeva, J.P. Katsoudas, and C.U. Segre, *J. Phys. Chem.* **C 117**, 18904 (2013).

Fit example: -225 mV without methanol

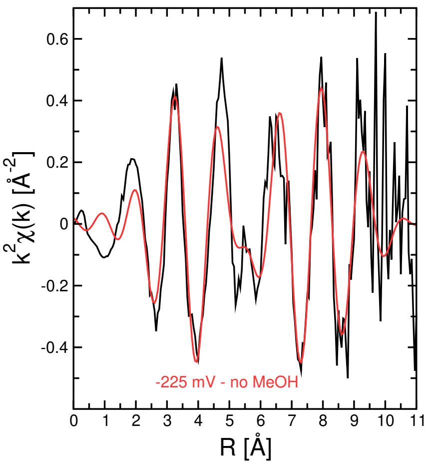

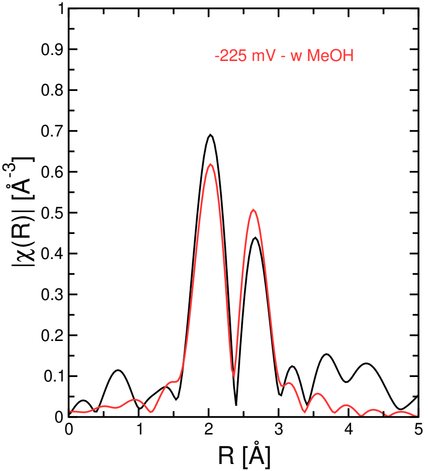

"In situ Ru K-Edge x-ray absorption spectroscopy study of methanol oxidation mechanisms on model submonolayer Ru on Pt nanoparticle electrocatalyst," C.J. Pelliccione, E.V. Timofeeva, J.P. Katsoudas, and C.U. Segre, *J. Phys. Chem.* **C 117**, 18904 (2013).

Fit example: 675 mV without methanol

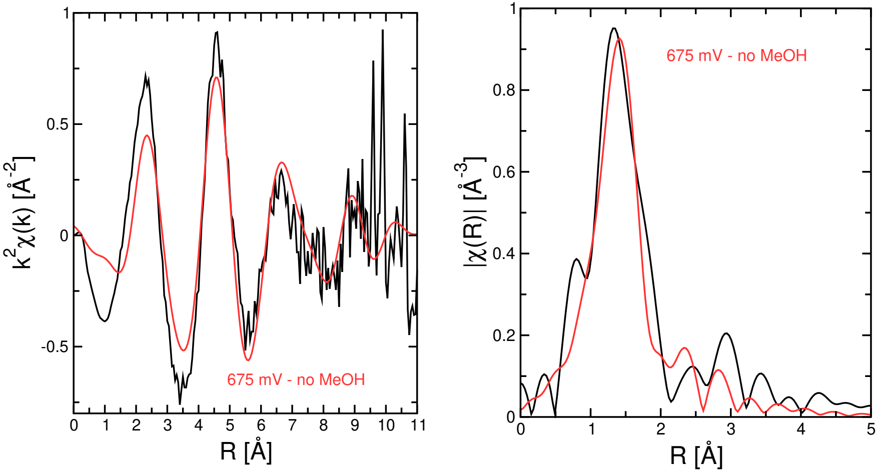

"In situ Ru K-Edge x-ray absorption spectroscopy study of methanol oxidation mechanisms on model submonolayer Ru on Pt nanoparticle electrocatalyst," C.J. Pelliccione, E.V. Timofeeva, J.P. Katsoudas, and C.U. Segre, *J. Phys. Chem.* **C 117**, 18904 (2013).

Fit example: 675 mV with methanol

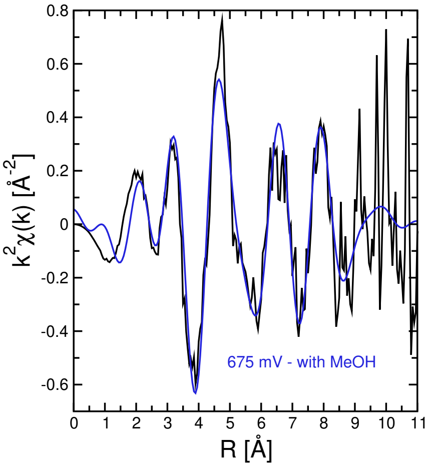

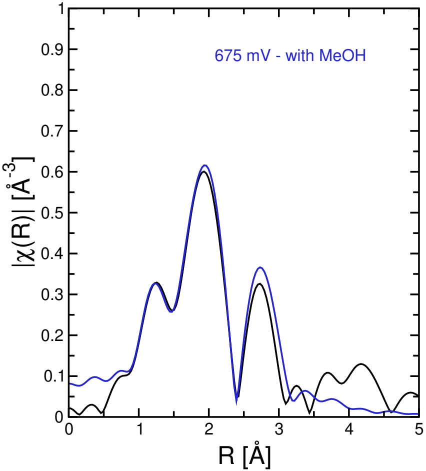

"In situ Ru K-Edge x-ray absorption spectroscopy study of methanol oxidation mechanisms on model submonolayer Ru on Pt nanoparticle electrocatalyst," C.J. Pelliccione, E.V. Timofeeva, J.P. Katsoudas, and C.U. Segre, *J. Phys. Chem.* **C 117**, 18904 (2013).

Ru-M paths

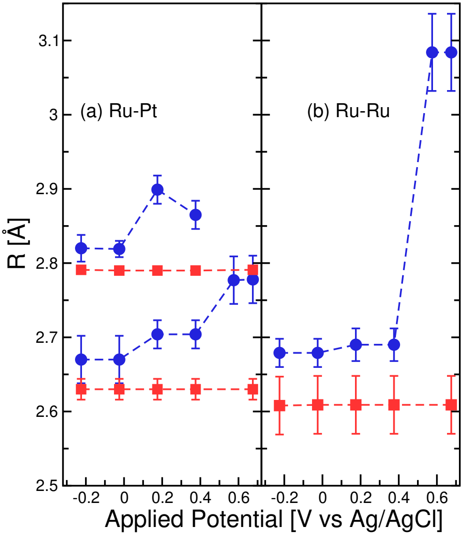

Without methanol

With methanol

"In situ Ru K-Edge x-ray absorption spectroscopy study of methanol oxidation mechanisms on model submonolayer Ru on Pt nanoparticle electrocatalyst," C.J. Pelliccione, E.V. Timofeeva, J.P. Katsoudas, and C.U. Segre, *J. Phys. Chem.* **C 117**, 18904 (2013).

Ru-M paths

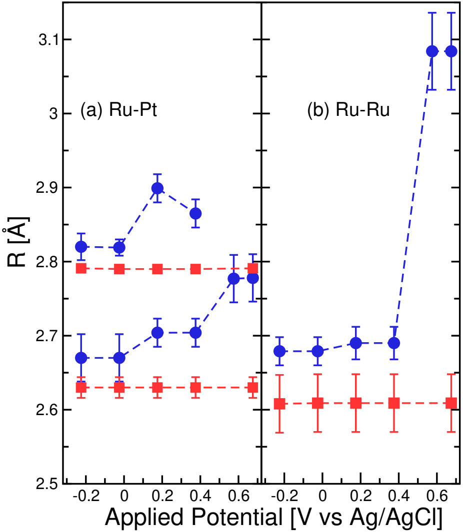

Without methanol

Ru-M distances are longer and RuO_2 is formed at high potentials

With methanol

"In situ Ru K-Edge x-ray absorption spectroscopy study of methanol oxidation mechanisms on model submonolayer Ru on Pt nanoparticle electrocatalyst," C.J. Pelliccione, E.V. Timofeeva, J.P. Katsoudas, and C.U. Segre, *J. Phys. Chem.* **C 117**, 18904 (2013).

Ru-M paths

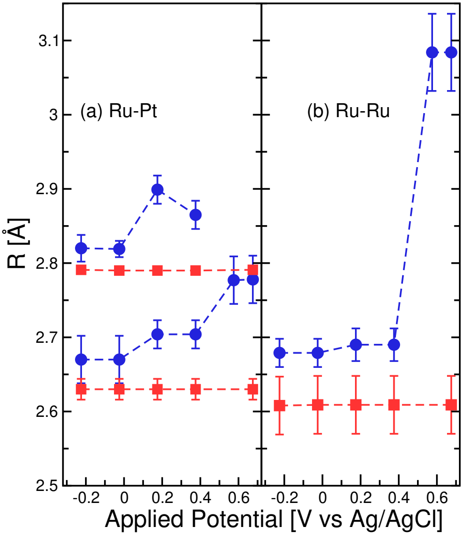

Without methanol

Ru-M distances are longer and RuO_2 is formed at high potentials

With methanol

Ru-M distances are shorter and remain the same at all potentials

"In situ Ru K-Edge x-ray absorption spectroscopy study of methanol oxidation mechanisms on model submonolayer Ru on Pt nanoparticle electrocatalyst," C.J. Pelliccione, E.V. Timofeeva, J.P. Katsoudas, and C.U. Segre, *J. Phys. Chem.* **C 117**, 18904 (2013).

Ru-O/C paths

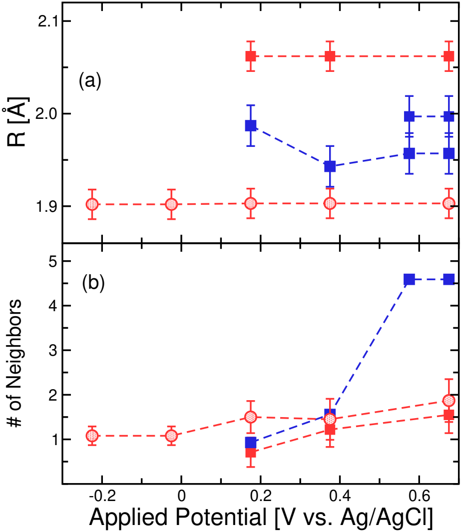

Without methanol

With methanol

"In situ Ru K-Edge x-ray absorption spectroscopy study of methanol oxidation mechanisms on model submonolayer Ru on Pt nanoparticle electrocatalyst," C.J. Pelliccione, E.V. Timofeeva, J.P. Katsoudas, and C.U. Segre, *J. Phys. Chem.* **C 117**, 18904 (2013).

Ru-O/C paths

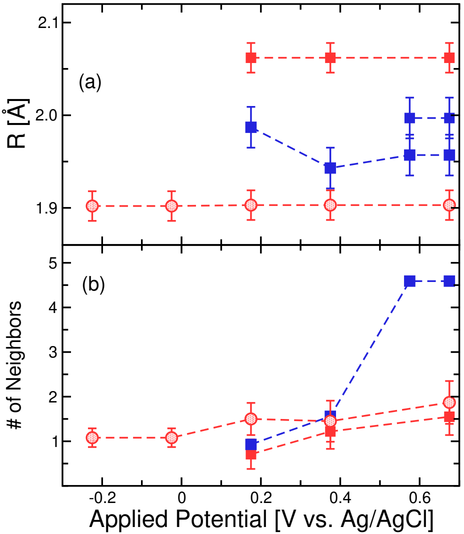

Without methanol

Above 375 mV Ru-O paths appear and total number of Ru-O neighbors increases to that of RuO_2

With methanol

"In situ Ru K-Edge x-ray absorption spectroscopy study of methanol oxidation mechanisms on model submonolayer Ru on Pt nanoparticle electrocatalyst," C.J. Pelliccione, E.V. Timofeeva, J.P. Katsoudas, and C.U. Segre, *J. Phys. Chem.* **C 117**, 18904 (2013).

Ru-O/C paths

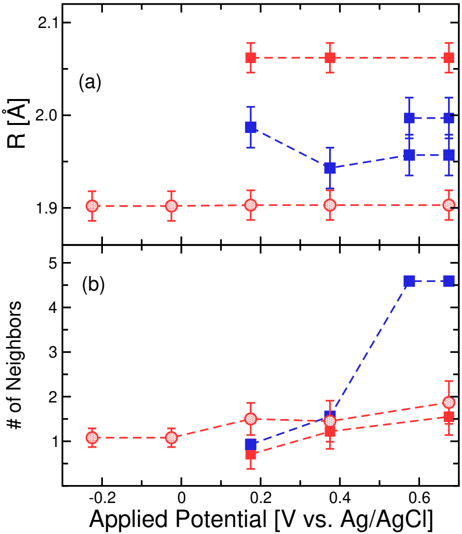

Without methanol

Above 375 mV Ru-O paths appear and total number of Ru-O neighbors increases to that of RuO_2

With methanol

Ru has one low Z neighbor at all potentials (carbon); a second above 175 mV (oxygen) with constant bond lengths and slightly increasing numbers

"In situ Ru K-Edge x-ray absorption spectroscopy study of methanol oxidation mechanisms on model submonolayer Ru on Pt nanoparticle electrocatalyst," C.J. Pelliccione, E.V. Timofeeva, J.P. Katsoudas, and C.U. Segre, *J. Phys. Chem.* **C 117**, 18904 (2013).

Bi-functional mechanism

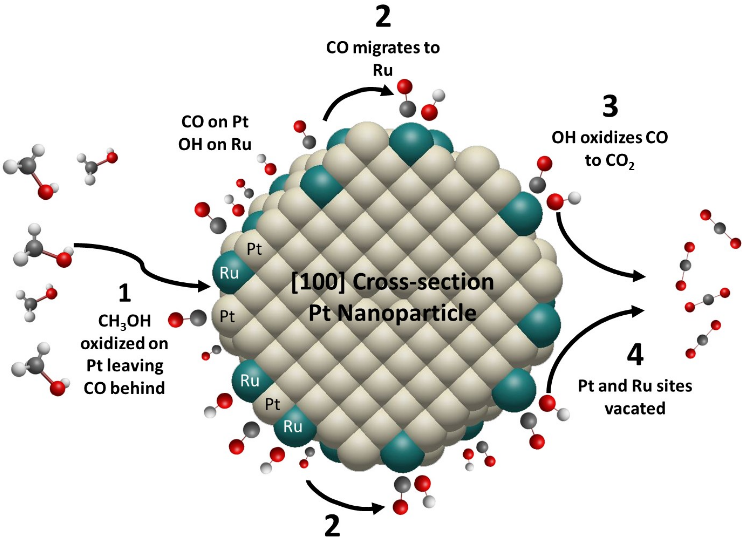

"In situ Ru K-Edge x-ray absorption spectroscopy study of methanol oxidation mechanisms on model submonolayer Ru on Pt nanoparticle electrocatalyst," C.J. Pelliccione, E.V. Timofeeva, J.P. Katsoudas, and C.U. Segre, *J. Phys. Chem.* **C 117**, 18904 (2013).

Today's outline - March 31, 2020 (part B)

Today's outline - March 31, 2020 (part B)

- Reversibility in tin anode battery materials

Today's outline - March 31, 2020 (part B)

- Reversibility in tin anode battery materials
    1. Modeling lithated Sn EXAFS

Today's outline - March 31, 2020 (part B)

- Reversibility in tin anode battery materials
  1. Modeling lithated Sn EXAFS
  2. The Sn lithiation process

Today's outline - March 31, 2020 (part B)

- Reversibility in tin anode battery materials
  1. Modeling lithated Sn EXAFS
  2. The Sn lithiation process
  3. Fully reversible lithiation of Sn phosphide

Initial *in situ* Sn-based anode EXAFS

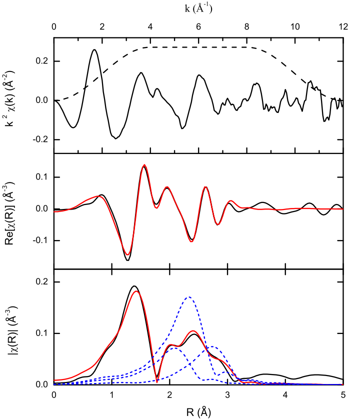

$Li_{22}Sn_5$ has 14 Sn-Li paths with distance of 3.4 Å or less. Model with three Sn-Li paths at “center of mass” locations

“In situ XAS study of the capacity fading mechanism in hybrid $Sn_3O_2(OH)_2$/graphite battery anode nanomaterials,” C.J. Pelliccione, E.V. Timofeeva, and C.U. Segre, *Chem. Mater.* **27**, 574-580 (2015).

Initial *in situ* Sn-based anode EXAFS

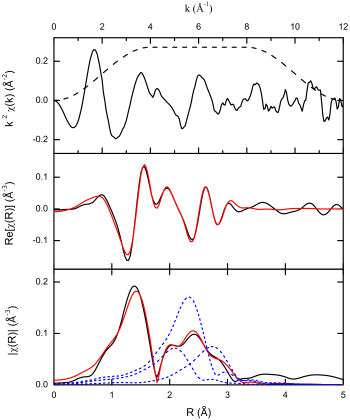

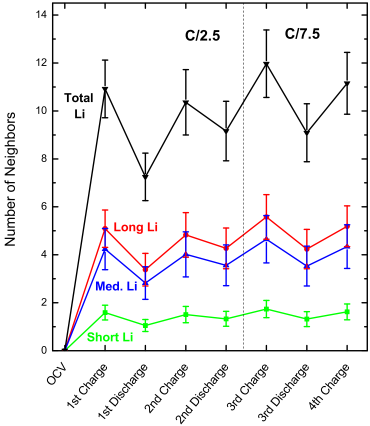

$Li_{22}Sn_5$ has 14 Sn-Li paths with distance of 3.4 Å or less. Model with three Sn-Li paths at "center of mass" locations

"In situ XAS study of the capacity fading mechanism in hybrid $Sn_3O_2(OH)_2$/graphite battery anode nanomaterials," C.J. Pelliccione, E.V. Timofeeva, and C.U. Segre, *Chem. Mater.* **27**, 574-580 (2015).

Sn nanoparticles – EXAFS versus potential

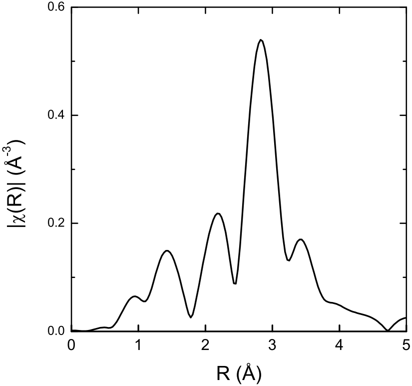

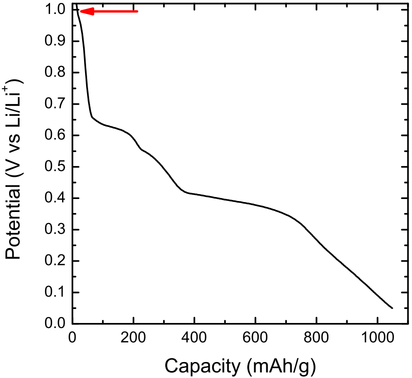

"Potential-resolved in situ x-ray absorption spectroscopy study of Sn and SnO_2 nanomaterial anodes for lithium-ion batteries," C.J. Pelliccione, E.V. Timofeeva, and C.U. Segre, *J. Phys. Chem. C* **120**, 5331-5339 (2016).

Sn nanoparticles – EXAFS versus potential

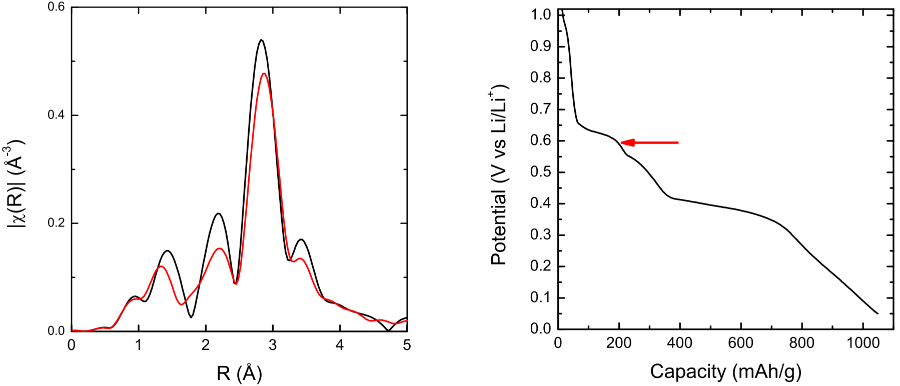

"Potential-resolved in situ x-ray absorption spectroscopy study of Sn and SnO_2 nanomaterial anodes for lithium-ion batteries," C.J. Pelliccione, E.V. Timofeeva, and C.U. Segre, *J. Phys. Chem. C* **120**, 5331-5339 (2016).

Sn nanoparticles – EXAFS versus potential

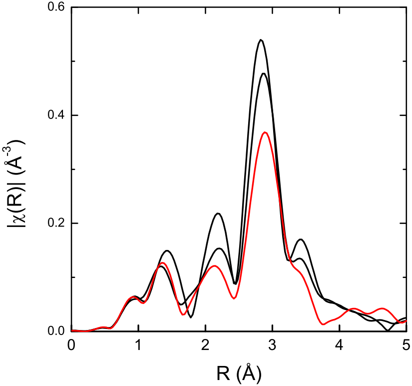

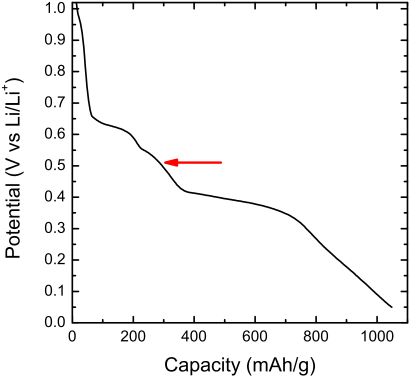

"Potential-resolved in situ x-ray absorption spectroscopy study of Sn and SnO_2 nanomaterial anodes for lithium-ion batteries," C.J. Pelliccione, E.V. Timofeeva, and C.U. Segre, *J. Phys. Chem. C* **120**, 5331-5339 (2016).

Sn nanoparticles – EXAFS versus potential

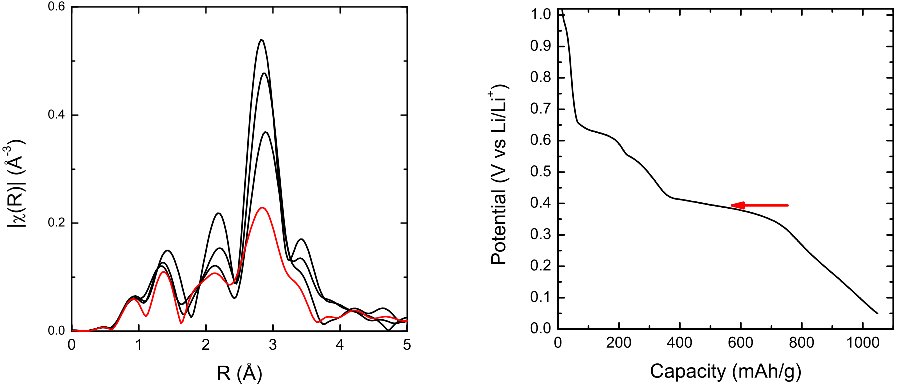

"Potential-resolved in situ x-ray absorption spectroscopy study of Sn and SnO_2 nanomaterial anodes for lithium-ion batteries," C.J. Pelliccione, E.V. Timofeeva, and C.U. Segre, *J. Phys. Chem. C* **120**, 5331-5339 (2016).

Sn nanoparticles – EXAFS versus potential

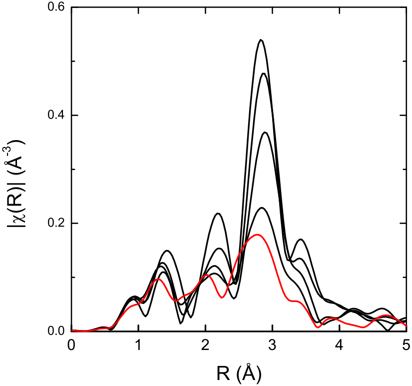

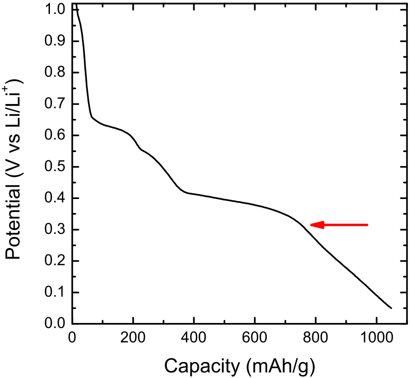

"Potential-resolved in situ x-ray absorption spectroscopy study of Sn and SnO_2 nanomaterial anodes for lithium-ion batteries," C.J. Pelliccione, E.V. Timofeeva, and C.U. Segre, *J. Phys. Chem. C* **120**, 5331-5339 (2016).

Sn nanoparticles – EXAFS versus potential

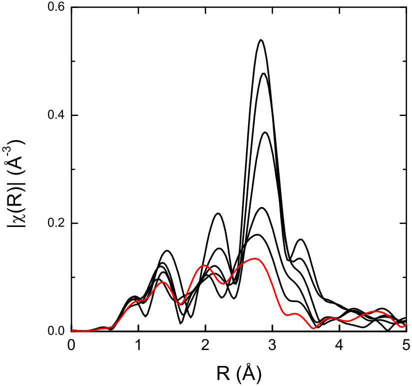

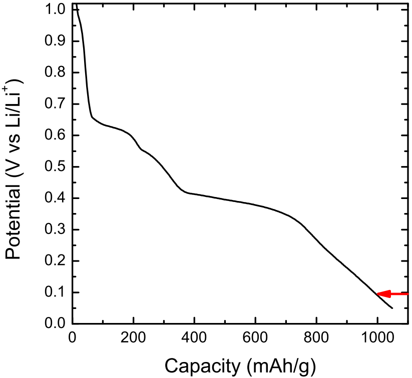

"Potential-resolved in situ x-ray absorption spectroscopy study of Sn and SnO_2 nanomaterial anodes for lithium-ion batteries," C.J. Pelliccione, E.V. Timofeeva, and C.U. Segre, *J. Phys. Chem. C* **120**, 5331-5339 (2016).

The Sn lithiation process

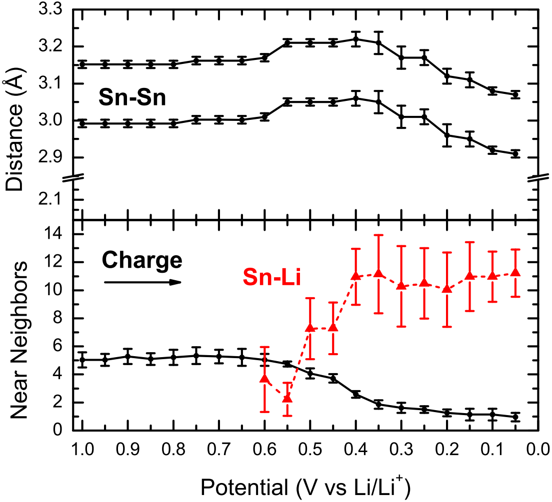

0.60V – Sn metal begins to break down and Li appears

0.45V – number of Li reaches 11 and stabilizes at near full $Li_{22}Sn_5$

However, Sn fades rapidly due to electric conductivity loss. What can be improved?

"Potential-resolved in situ x-ray absorption spectroscopy study of Sn and SnO_2 nanomaterial anodes for lithium-ion batteries," C.J. Pelliccione, E.V. Timofeeva, and C.U. Segre, *J. Phys. Chem. C* **120**, 5331-5339 (2016).

Sn_4P_3/graphite composite anode

Sn_4P_3 synthesized by high energy ball milling, then ball milled again with graphite to obtain composite

"In situ EXAFS-derived mechanism of highly reversible tin phosphide/graphite composite anode for Li-ion batteries," Y. Ding, Z. Li, E.V. Timofeeva, and C.U. Segre, *Adv. Energy Mater.* **8**, 1702134 (2018).

Sn_4P_3/graphite composite anode

Sn_4P_3 synthesized by high energy ball milling, then ball milled again with graphite to obtain composite

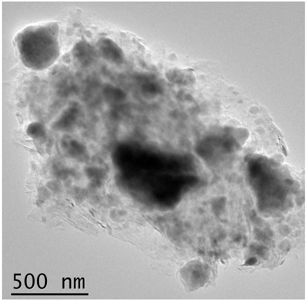

"In situ EXAFS-derived mechanism of highly reversible tin phosphide/graphite composite anode for Li-ion batteries," Y. Ding, Z. Li, E.V. Timofeeva, and C.U. Segre, *Adv. Energy Mater.* **8**, 1702134 (2018).

Sn_4P_3/graphite composite anode

Sn_4P_3 synthesized by high energy ball milling, then ball milled again with graphite to obtain composite

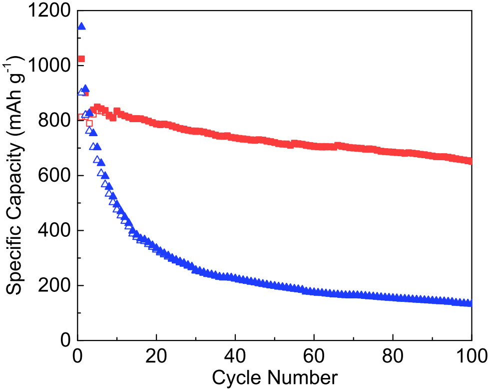

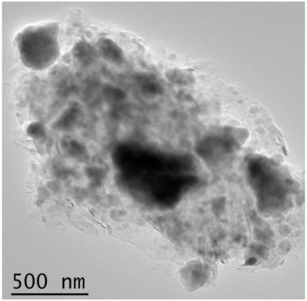

"In situ EXAFS-derived mechanism of highly reversible tin phosphide/graphite composite anode for Li-ion batteries," Y. Ding, Z. Li, E.V. Timofeeva, and C.U. Segre, *Adv. Energy Mater.* **8**, 1702134 (2018).

Sn_4P_3/graphite composite anode

Sn_4P_3 synthesized by high energy ball milling, then ball milled again with graphite to obtain composite

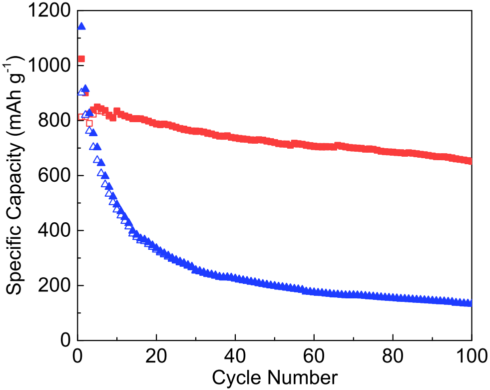

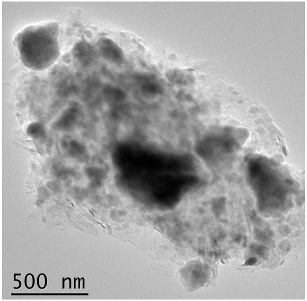

Sn_4P_3/graphite composite shows stable, reversible capacity of 610 mAh/g for 100 cycles at C/2 compared to rapidly fading pure Sn_4P_3 material.

"In situ EXAFS-derived mechanism of highly reversible tin phosphide/graphite composite anode for Li-ion batteries," Y. Ding, Z. Li, E.V. Timofeeva, and C.U. Segre, *Adv. Energy Mater.* **8**, 1702134 (2018).

In situ EXAFS of Sn_4P_3/graphite

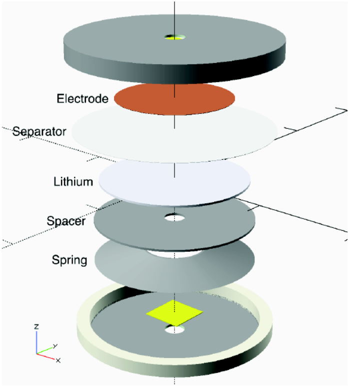

“In situ EXAFS-derived mechanism of highly reversible tin phosphide/graphite composite anode for Li-ion batteries,” Y. Ding, Z. Li, E.V. Timofeeva, and C.U. Segre, *Adv. Energy Mater.* **8**, 1702134 (2018).

In situ EXAFS of Sn_4P_3/graphite

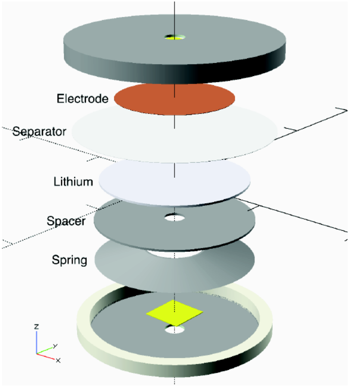

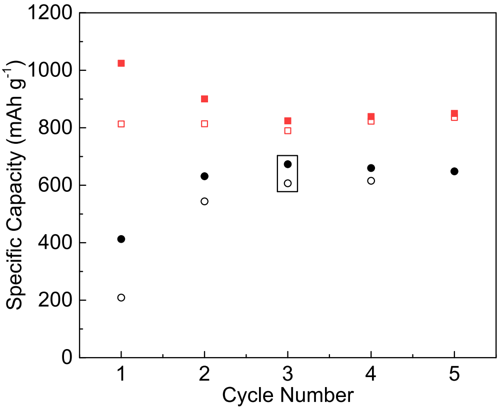

"In situ EXAFS-derived mechanism of highly reversible tin phosphide/graphite composite anode for Li-ion batteries," Y. Ding, Z. Li, E.V. Timofeeva, and C.U. Segre, *Adv. Energy Mater.* **8**, 1702134 (2018).

In situ EXAFS of Sn_4P_3/graphite

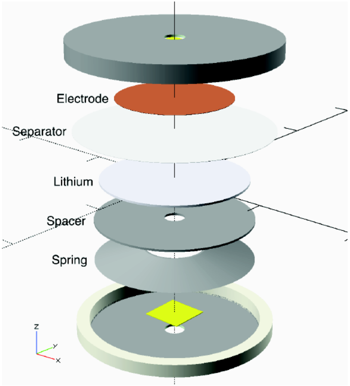

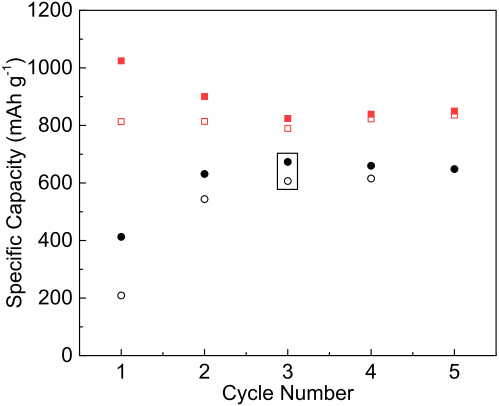

Results for *in situ* coin cell are close to the capacity of the unmodified cell at C/4, indicating good reversibility by the 3rd cycle.

"In situ EXAFS-derived mechanism of highly reversible tin phosphide/graphite composite anode for Li-ion batteries," Y. Ding, Z. Li, E.V. Timofeeva, and C.U. Segre, *Adv. Energy Mater.* **8**, 1702134 (2018).

Third cycle comparison

By the third lithiation and third delithiation, the difference between pure Sn_4P_3 and the Sn_4P_3/graphite composite is clear.

“In situ EXAFS-derived mechanism of highly reversible tin phosphide/graphite composite anode for Li-ion batteries,” Y. Ding, Z. Li, E.V. Timofeeva, and C.U. Segre, *Adv. Energy Mater.* **8**, 1702134 (2018).

Third cycle comparison

By the third lithiation and third delithiation, the difference between pure Sn_4P_3 and the Sn_4P_3/graphite composite is clear.

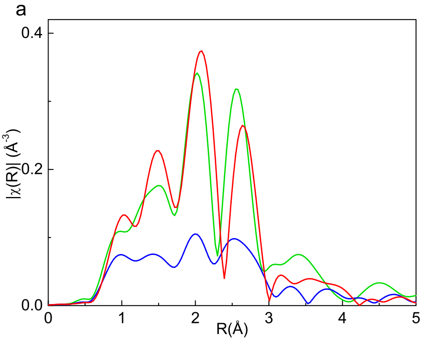

Sn_4P_3/graphite composite

"In situ EXAFS-derived mechanism of highly reversible tin phosphide/graphite composite anode for Li-ion batteries," Y. Ding, Z. Li, E.V. Timofeeva, and C.U. Segre, *Adv. Energy Mater.* **8**, 1702134 (2018).

Third cycle comparison

By the third lithiation and third delithiation, the difference between pure Sn_4P_3 and the Sn_4P_3/graphite composite is clear.

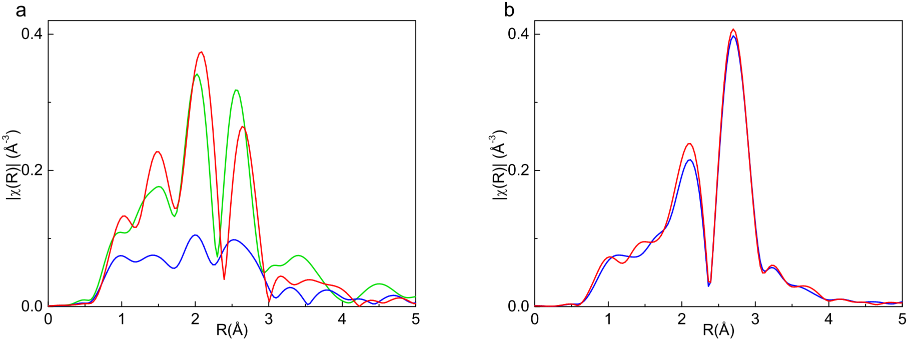

Sn_4P_3/graphite composite

pure Sn_4P_3

"In situ EXAFS-derived mechanism of highly reversible tin phosphide/graphite composite anode for Li-ion batteries," Y. Ding, Z. Li, E.V. Timofeeva, and C.U. Segre, *Adv. Energy Mater.* **8**, 1702134 (2018).

Third cycle comparison

By the third lithiation and third delithiation, the difference between pure Sn_4P_3 and the Sn_4P_3/graphite composite is clear.

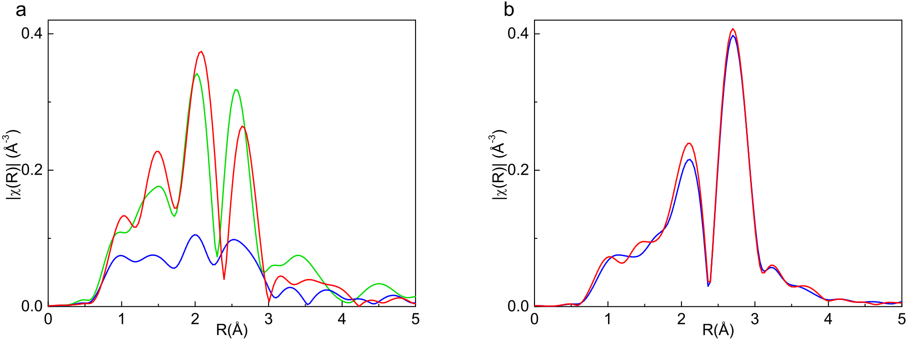

Sn_4P_3/graphite composite

pure Sn_4P_3

Even at the 100th delithiation, the Sn_4P_3/graphite composite measured *ex situ* is showing the same features as at the 3rd cycle.

"In situ EXAFS-derived mechanism of highly reversible tin phosphide/graphite composite anode for Li-ion batteries," Y. Ding, Z. Li, E.V. Timofeeva, and C.U. Segre, *Adv. Energy Mater.* **8**, 1702134 (2018).

Example fits

Fit EXAFS for bond lengths and coordination numbers

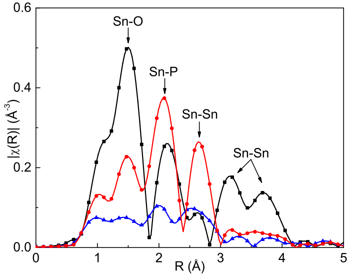

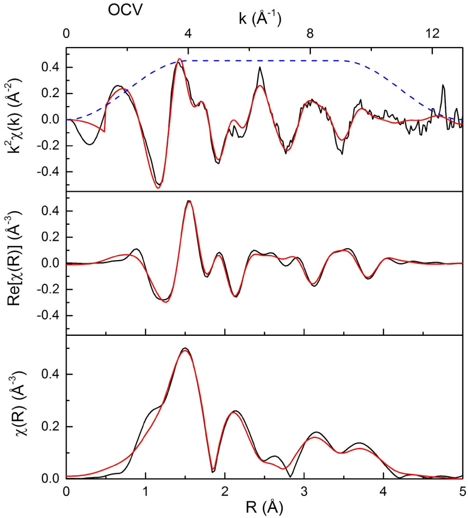

The Sn-O peak at OCV is due to ball milling, which introduces oxygen.

"In situ EXAFS-derived mechanism of highly reversible tin phosphide/graphite composite anode for Li-ion batteries," Y. Ding, Z. Li, E.V. Timofeeva, and C.U. Segre, *Adv. Energy Mater.* **8**, 1702134 (2018).

Example fits

Fit EXAFS for bond lengths and coordination numbers

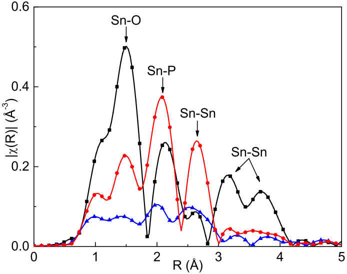

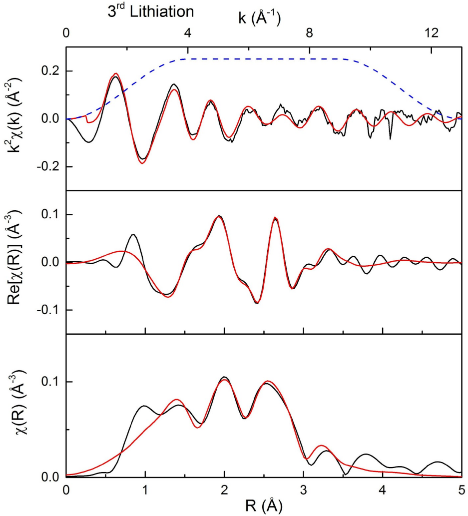

By the 3*rd* lithiated state, the EXAFS is dominated by Sn-Li paths at 2.7 Å and 3.0 Å.

"In situ EXAFS-derived mechanism of highly reversible tin phosphide/graphite composite anode for Li-ion batteries," Y. Ding, Z. Li, E.V. Timofeeva, and C.U. Segre, *Adv. Energy Mater.* **8**, 1702134 (2018).

Example fits

Fit EXAFS for bond lengths and coordination numbers

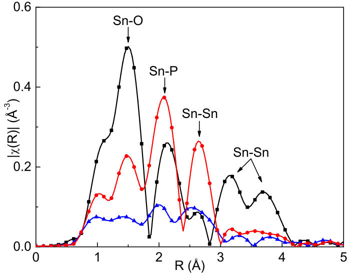

At the 3rd delithiation, the Sn-P path reappears but at a shorter distance, in an amorphous SnP$_x$ phase.

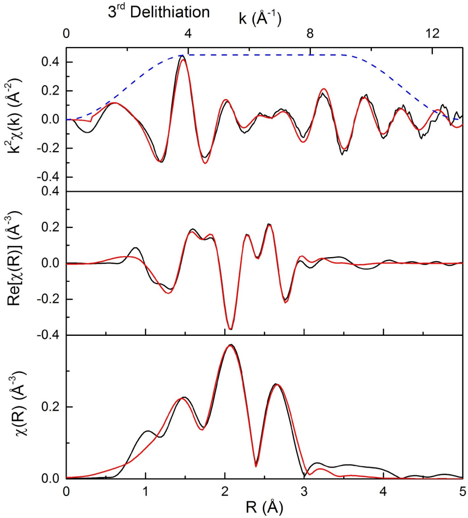

"In situ EXAFS-derived mechanism of highly reversible tin phosphide/graphite composite anode for Li-ion batteries," Y. Ding, Z. Li, E.V. Timofeeva, and C.U. Segre, *Adv. Energy Mater.* **8**, 1702134 (2018).

Sn_4P_3/graphite path lengths

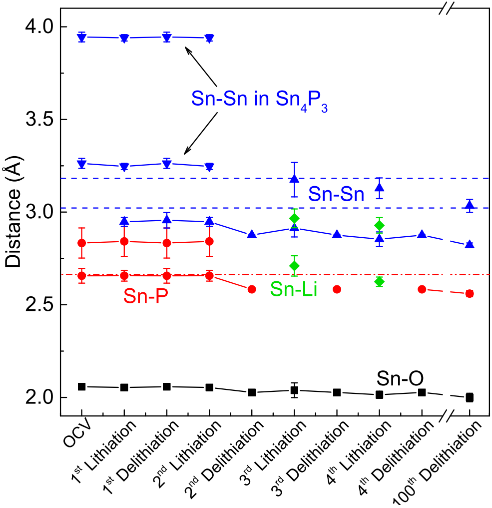

Y. Ding et al., "In situ EXAFS-derived mechanism of highly reversible tin phosphide/graphite composite anode for Li-ion batteries," Y. Ding, Z. Li, E.V. Timofeeva, and C.U. Segre, *Adv. Energy Mater.* **8**, 1702134 (2018).

Sn_4P_3/graphite path lengths

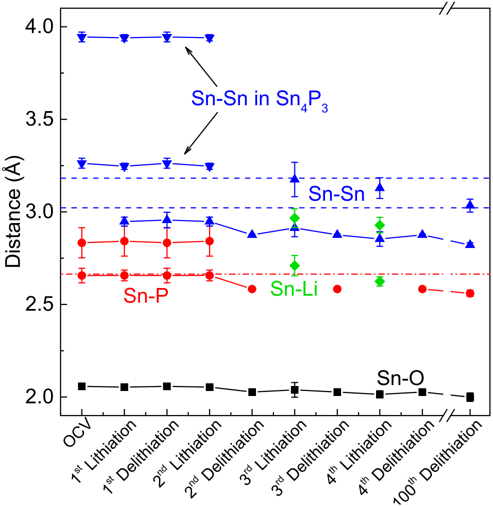

Sn-Sn distance close to those of metallic Sn indicate the presence of small Sn clusters which may never fully lithiate

Y. Ding et al., "In situ EXAFS-derived mechanism of highly reversible tin phosphide/graphite composite anode for Li-ion batteries," Y. Ding, Z. Li, E.V. Timofeeva, and C.U. Segre, *Adv. Energy Mater.* **8**, 1702134 (2018).

Sn_4P_3/graphite path lengths

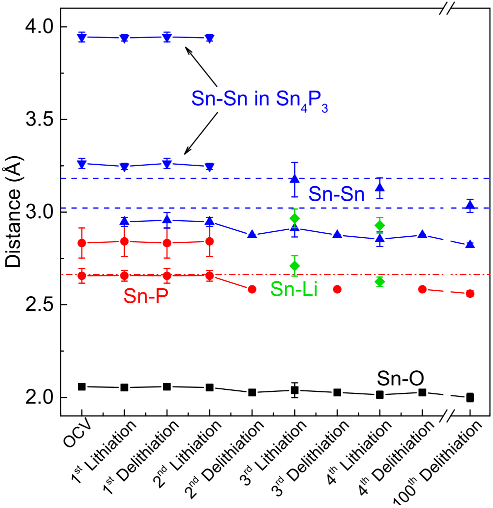

Sn-Sn distance close to those of metallic Sn indicate the presence of small Sn clusters which may never fully lithiate

Longer Sn-P distance characteristic of Sn_4P_3 is gone after initial conversion to the SnP_x amorphous phase is complete

Y. Ding et al., "In situ EXAFS-derived mechanism of highly reversible tin phosphide/graphite composite anode for Li-ion batteries," Y. Ding, Z. Li, E.V. Timofeeva, and C.U. Segre, *Adv. Energy Mater.* **8**, 1702134 (2018).

Sn_4P_3/graphite path lengths

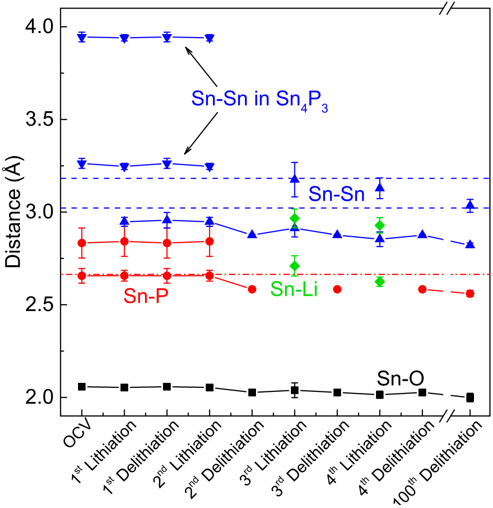

Sn-Sn distance close to those of metallic Sn indicate the presence of small Sn clusters which may never fully lithiate

Longer Sn-P distance characteristic of Sn_4P_3 is gone after initial conversion to the SnP_x amorphous phase is complete

Only 2 Sn-Li paths present in this material

Y. Ding et al., "In situ EXAFS-derived mechanism of highly reversible tin phosphide/graphite composite anode for Li-ion batteries," Y. Ding, Z. Li, E.V. Timofeeva, and C.U. Segre, *Adv. Energy Mater.* **8**, 1702134 (2018).

Sn_4P_3/graphite path lengths

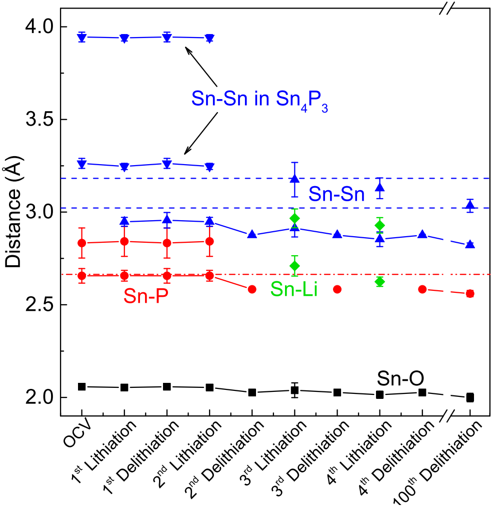

Sn-Sn distance close to those of metallic Sn indicate the presence of small Sn clusters which may never fully lithiate

Longer Sn-P distance characteristic of Sn_4P_3 is gone after initial conversion to the SnP_x amorphous phase is complete

Only 2 Sn-Li paths present in this material

Sn-O distances remain constant, likely indicative of surface contamination

Y. Ding et al., "In situ EXAFS-derived mechanism of highly reversible tin phosphide/graphite composite anode for Li-ion batteries," Y. Ding, Z. Li, E.V. Timofeeva, and C.U. Segre, *Adv. Energy Mater.* **8**, 1702134 (2018).

Sn_4P_3/graphite coordination numbers

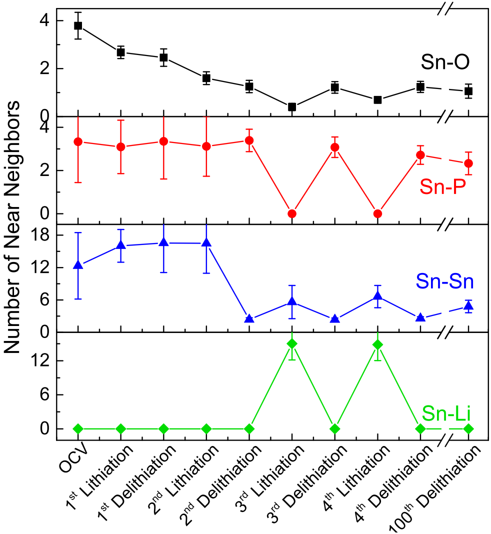

Y. Ding et al., "In situ EXAFS-derived mechanism of highly reversible tin phosphide/graphite composite anode for Li-ion batteries," Y. Ding, Z. Li, E.V. Timofeeva, and C.U. Segre, *Adv. Energy Mater.* **8**, 1702134 (2018).

Sn_4P_3/graphite coordination numbers

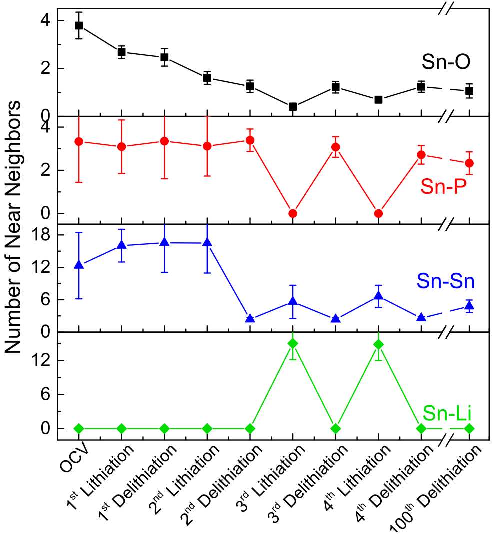

Sn-O neighbors decrease quickly, remaining small and partially reversible up to 100 cycles

Y. Ding et al., "In situ EXAFS-derived mechanism of highly reversible tin phosphide/graphite composite anode for Li-ion batteries," Y. Ding, Z. Li, E.V. Timofeeva, and C.U. Segre, *Adv. Energy Mater.* **8**, 1702134 (2018).

Sn_4P_3/graphite coordination numbers

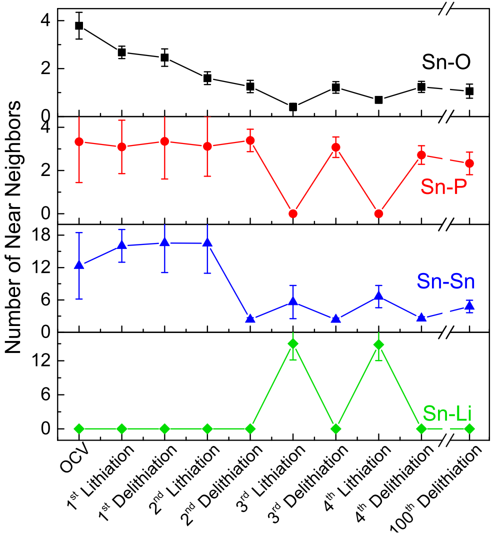

Sn-O neighbors decrease quickly, remaining small and partially reversible up to 100 cycles

Sn-P reversible after initial conversion with a slow decrease which correlates to capacity loss

Y. Ding et al., "In situ EXAFS-derived mechanism of highly reversible tin phosphide/graphite composite anode for Li-ion batteries," Y. Ding, Z. Li, E.V. Timofeeva, and C.U. Segre, *Adv. Energy Mater.* **8**, 1702134 (2018).

Sn_4P_3/graphite coordination numbers

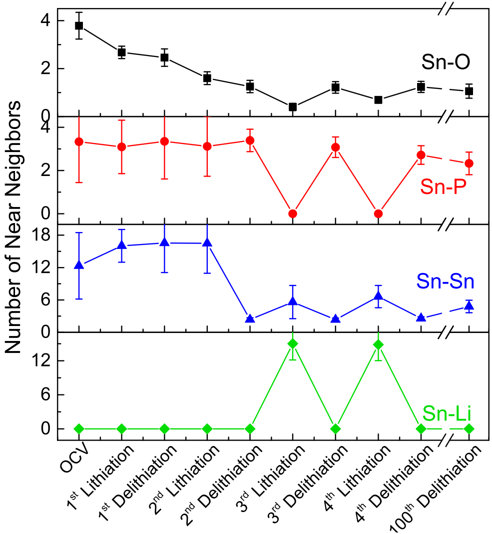

Sn-O neighbors decrease quickly, remaining small and partially reversible up to 100 cycles

Sn-P reversible after initial conversion with a slow decrease which correlates to capacity loss

Very small Sn-Sn metallic clusters present throughout

Y. Ding et al., "In situ EXAFS-derived mechanism of highly reversible tin phosphide/graphite composite anode for Li-ion batteries," Y. Ding, Z. Li, E.V. Timofeeva, and C.U. Segre, *Adv. Energy Mater.* **8**, 1702134 (2018).

Sn_4P_3/graphite coordination numbers

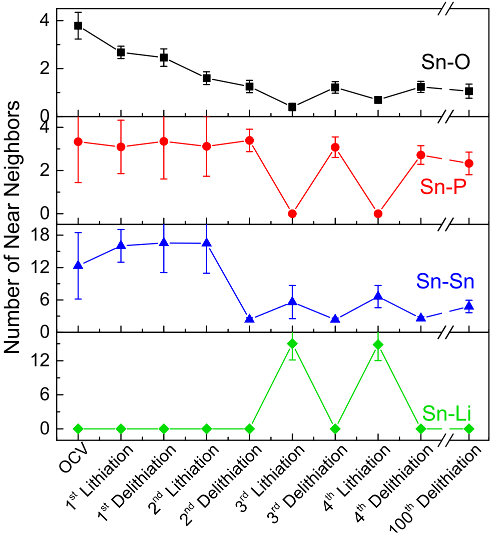

Sn-O neighbors decrease quickly, remaining small and partially reversible up to 100 cycles

Sn-P reversible after initial conversion with a slow decrease which correlates to capacity loss

Very small Sn-Sn metallic clusters present throughout

The ∼3.3 Sn-P neighbors in the delithiated state indicate a possibly tetrahedral Sn coordination in SnP_x

Y. Ding et al., "In situ EXAFS-derived mechanism of highly reversible tin phosphide/graphite composite anode for Li-ion batteries," Y. Ding, Z. Li, E.V. Timofeeva, and C.U. Segre, *Adv. Energy Mater.* **8**, 1702134 (2018).

Third cycle dynamic snapshot

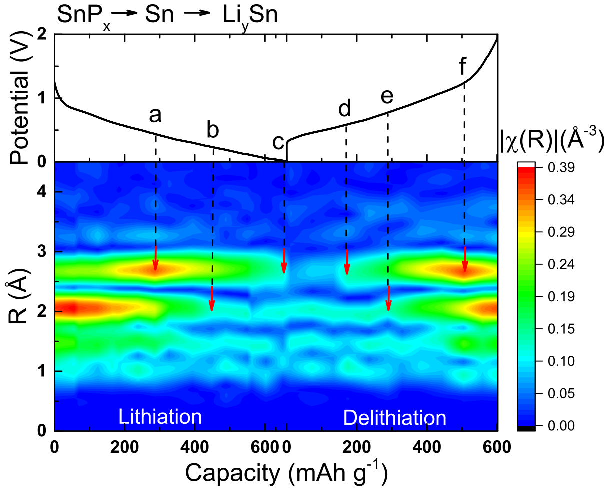

"In situ EXAFS-derived mechanism of highly reversible tin phosphide/graphite composite anode for Li-ion batteries," Y. Ding, Z. Li, E.V. Timofeeva, and C.U. Segre, *Adv. Energy Mater.* **8**, 1702134 (2018).

Third cycle dynamic snapshot

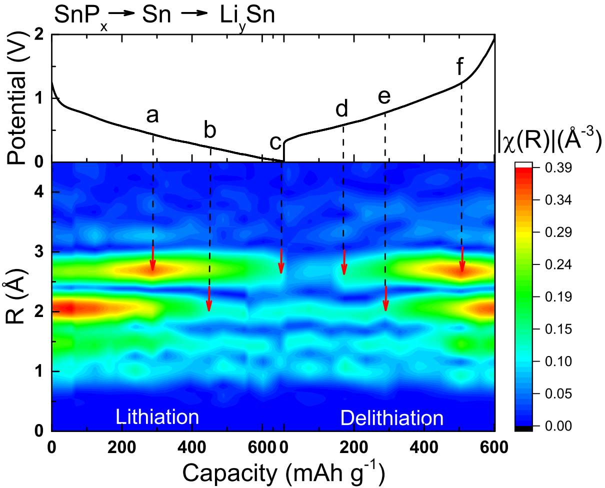

Amorphous SnP_x fully formed at start of 3^{rd} cycle

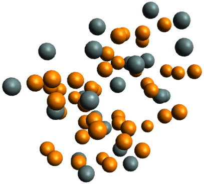

“In situ EXAFS-derived mechanism of highly reversible tin phosphide/graphite composite anode for Li-ion batteries,” Y. Ding, Z. Li, E.V. Timofeeva, and C.U. Segre, *Adv. Energy Mater.* **8**, 1702134 (2018).

Third cycle dynamic snapshot

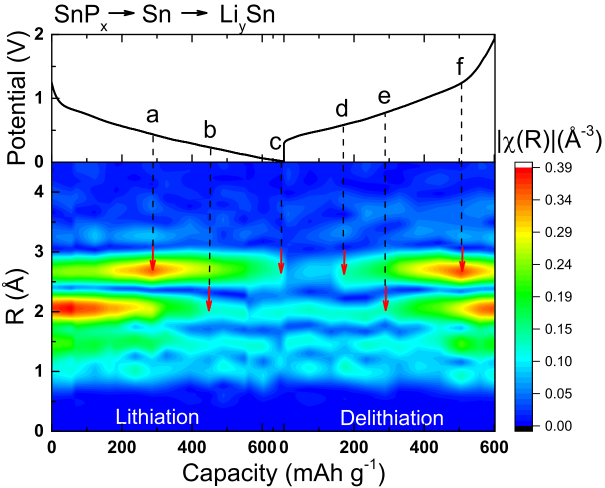

Amorphous SnP_x fully formed at start of 3^{rd} cvcle

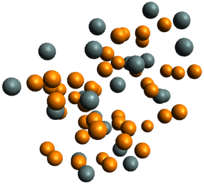

a. Sn lithiating

"In situ EXAFS-derived mechanism of highly reversible tin phosphide/graphite composite anode for Li-ion batteries," Y. Ding, Z. Li, E.V. Timofeeva, and C.U. Segre, *Adv. Energy Mater.* **8**, 1702134 (2018).

Third cycle dynamic snapshot

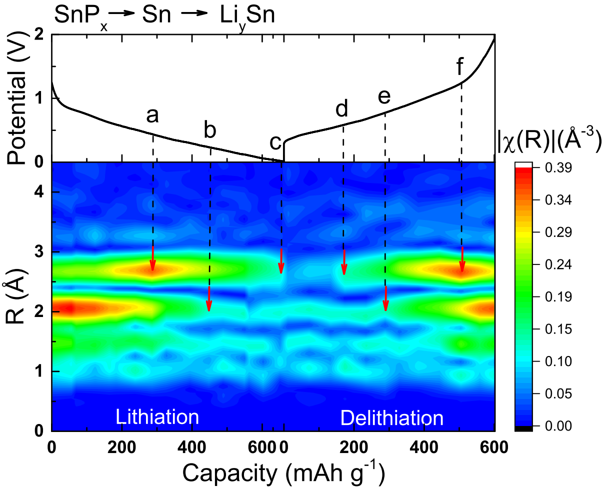

Amorphous SnP_x fully formed at start of 3^{rd} cvcle

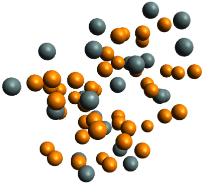

a. Sn lithiating
b. SnP_x all gone

"In situ EXAFS-derived mechanism of highly reversible tin phosphide/graphite composite anode for Li-ion batteries," Y. Ding, Z. Li, E.V. Timofeeva, and C.U. Segre, *Adv. Energy Mater.* **8**, 1702134 (2018).

Third cycle dynamic snapshot

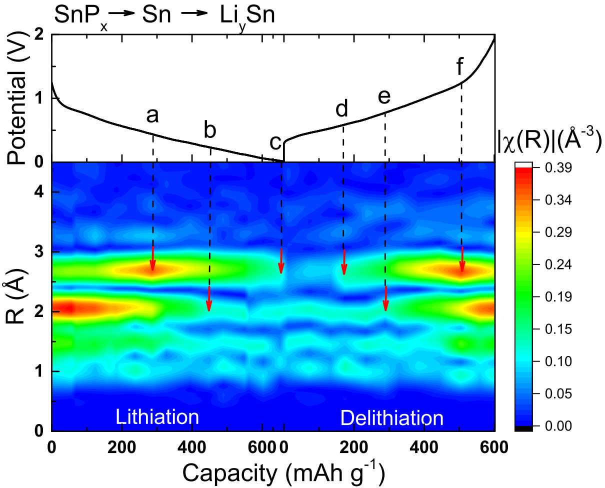

Amorphous SnP_x fully formed at start of 3^{rd} cvcle

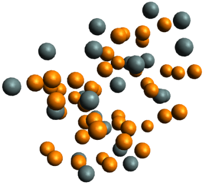

a. Sn lithiating
b. SnP_x all gone
c. full lithiation

"In situ EXAFS-derived mechanism of highly reversible tin phosphide/graphite composite anode for Li-ion batteries," Y. Ding, Z. Li, E.V. Timofeeva, and C.U. Segre, *Adv. Energy Mater.* **8**, 1702134 (2018).

Third cycle dynamic snapshot

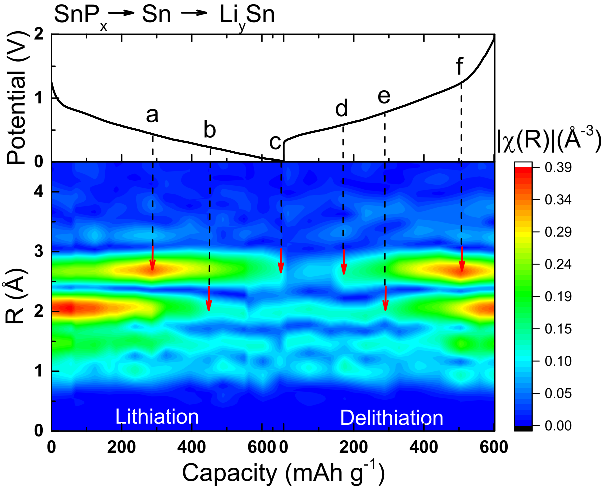

Amorphous SnP_x fully formed at start of 3rd cvcle

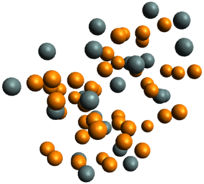

a. Sn lithiating
b. SnP_x all gone
c. full lithiation
d. Sn appears

"In situ EXAFS-derived mechanism of highly reversible tin phosphide/graphite composite anode for Li-ion batteries," Y. Ding, Z. Li, E.V. Timofeeva, and C.U. Segre, *Adv. Energy Mater.* **8**, 1702134 (2018).

Third cycle dynamic snapshot

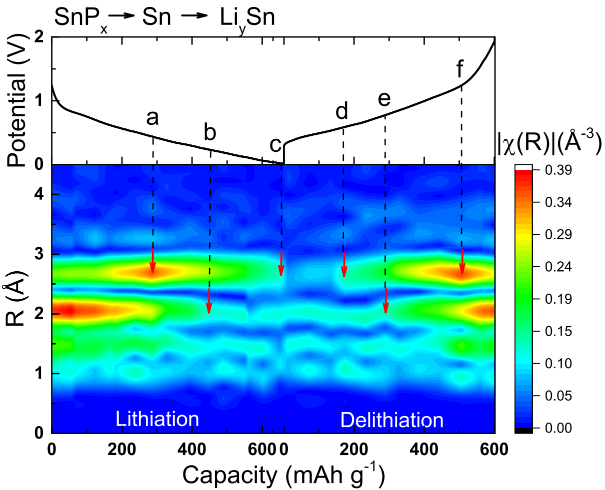

Amorphous SnP_x fully formed at start of 3rd cvcle

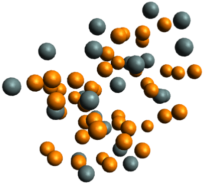

a. Sn lithiating
b. SnP_x all gone
c. full lithiation
d. Sn appears
e. SnP_x appears

"In situ EXAFS-derived mechanism of highly reversible tin phosphide/graphite composite anode for Li-ion batteries," Y. Ding, Z. Li, E.V. Timofeeva, and C.U. Segre, *Adv. Energy Mater.* **8**, 1702134 (2018).

Third cycle dynamic snapshot

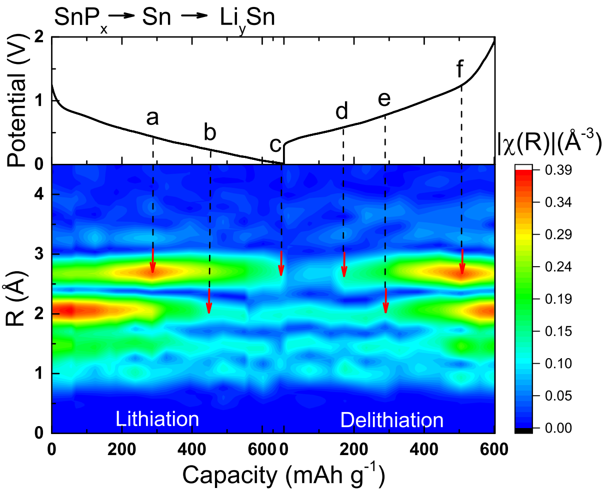

Amorphous SnP_x fully formed at start of 3^{rd} cvcle

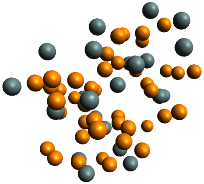

a. Sn lithiating
b. SnP_x all gone
c. full lithiation
d. Sn appears
e. SnP_x appears
f. Sn delithiated

"In situ EXAFS-derived mechanism of highly reversible tin phosphide/graphite composite anode for Li-ion batteries," Y. Ding, Z. Li, E.V. Timofeeva, and C.U. Segre, *Adv. Energy Mater.* **8**, 1702134 (2018).

Today's outline - March 31, 2020 (part C)

Today's outline - March 31, 2020 (part C)

- Clustering in oxide chromophores

Today's outline - March 31, 2020 (part C)

- Clustering in oxide chromophores

    1. $YMn_{1-x}In_xO_3$

Today's outline - March 31, 2020 (part C)

- Clustering in oxide chromophores
  1. $YMn_{1-x}In_xO_3$
  2. $YMn_{1-x}Ga_xO_3$

Chromophores based on $YInO_3$

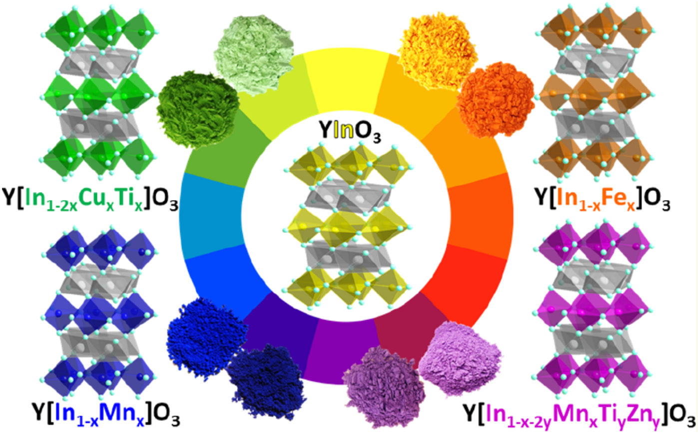

J. Li, S. Lorger, J.K. Stalick, A.W. Sleight, and M.A. Subramanian, *Inorg. Chem.* **55**, 9798–9804 (2016).

Chromophores based on $YInO_3$

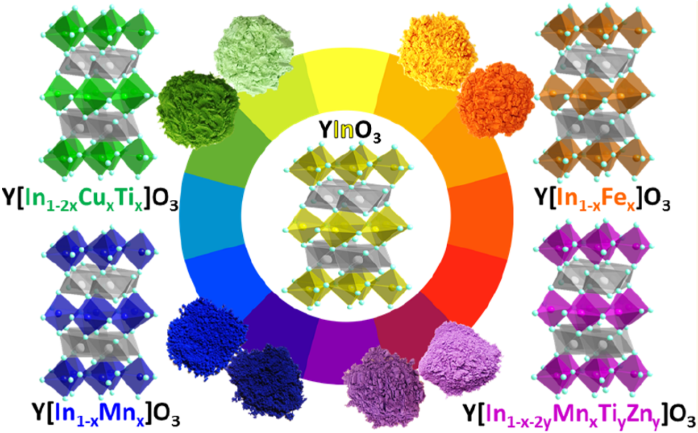

Base compound is white, dopant gives intense colors

J. Li, S. Lorger, J.K. Stalick, A.W. Sleight, and M.A. Subramanian, *Inorg. Chem.* **55**, 9798–9804 (2016).

Chromophores based on $YInO_3$

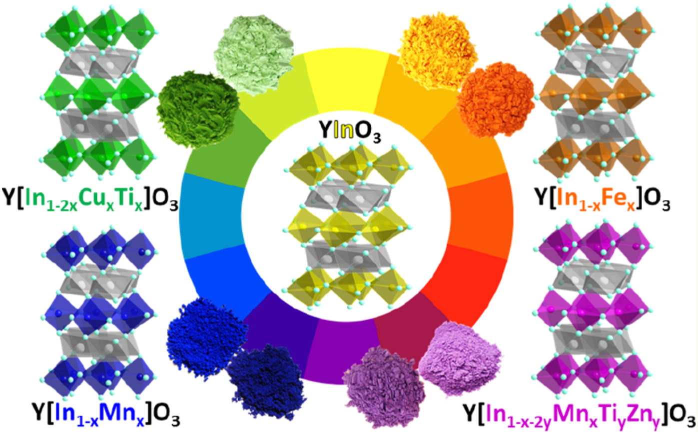

Base compound is white, dopant gives intense colors
The Mn variant has commercial promise

J. Li, S. Lorger, J.K. Stalick, A.W. Sleight, and M.A. Subramanian, *Inorg. Chem.* **55**, 9798–9804 (2016).

Chromophores based on $YInO_3$

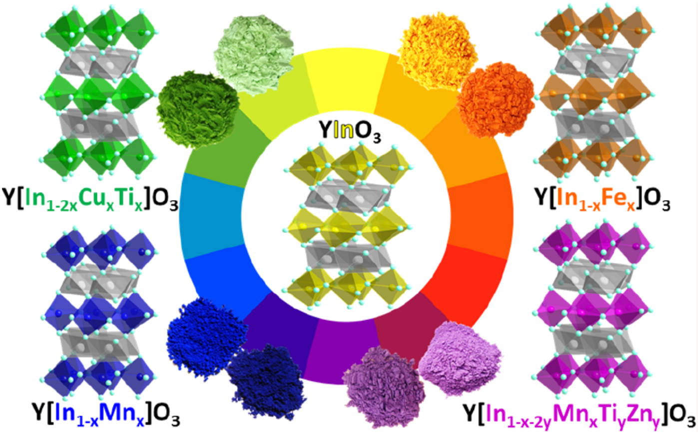

Base compound is white, dopant gives intense colors

The Mn variant has commercial promise

Hexagonal structure with YO_6 octahedra and InO_5 trigonal bipyramids

J. Li, S. Lorger, J.K. Stalick, A.W. Sleight, and M.A. Subramanian, *Inorg. Chem.* **55**, 9798–9804 (2016).

$YMn_{1-x}In_xO_3$ solid solution

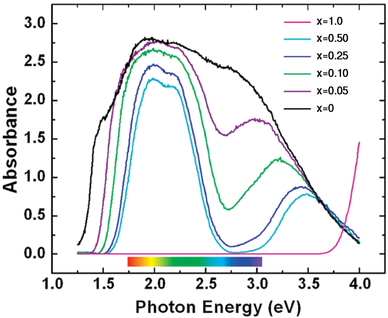

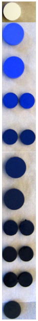

A.E. Smith, et al., *J. Am. Chem. Soc.* **131**, 17084-17086 (2009).

$YMn_{1-x}In_xO_3$ solid solution

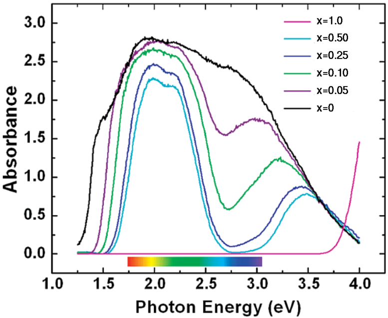

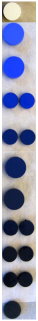

A.E. Smith, et al., *J. Am. Chem. Soc.* **131**, 17084-17086 (2009).

Color varies from bright blue to nearly black with optical absorption reflecting the same variation

$YMn_{1-x}In_xO_3$ solid solution

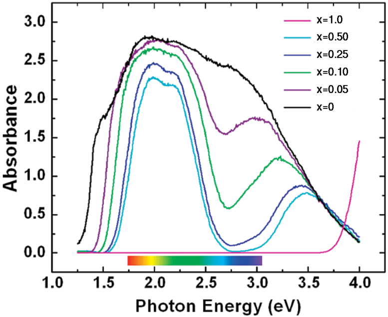

A.E. Smith, et al., *J. Am. Chem. Soc.* **131**, 17084-17086 (2009).

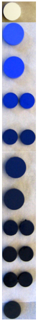

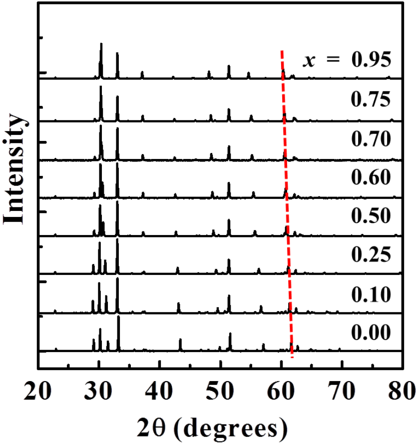

Color varies from bright blue to nearly black with optical absorption reflecting the same variation

YMn$_{1-x}$In$_x$O$_3$ solid solution

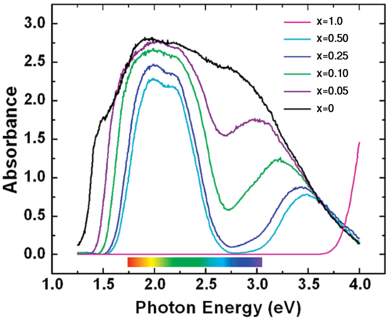

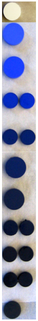

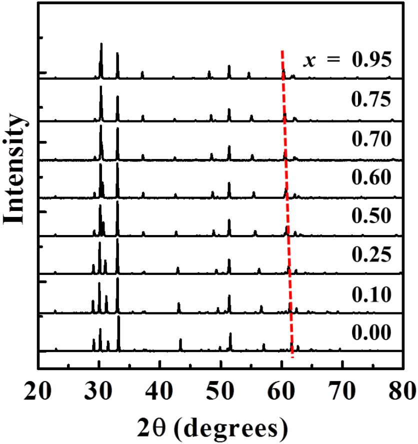

A.E. Smith, et al., *J. Am. Chem. Soc.* **131**, 17084-17086 (2009).

Color varies from bright blue to nearly black with optical absorption reflecting the same variation

Diffraction patterns show a continuous shift in peak position which is typical of uniform solid solutions

$YMn_{1-x}In_xO_3$ refinements

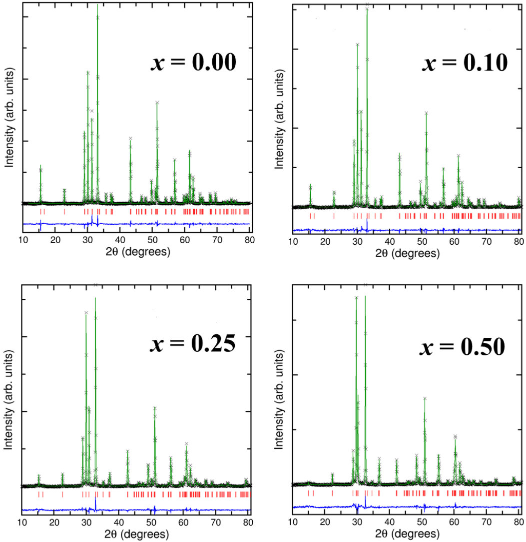

All samples are single phase

"Evolution of the local structure within chromophoric Mn-O_5 trigonal bipyramids in $YMn_{1-x}In_xO_3$ with composition," S. Mukherjee, H. Ganegoda, A. Kumar, S. Pal, C.U. Segre, and D.D. Sarma, *Inorg. Chem.* **57**, 9012–9019 (2018).

$YMn_{1-x}In_xO_3$ refinements

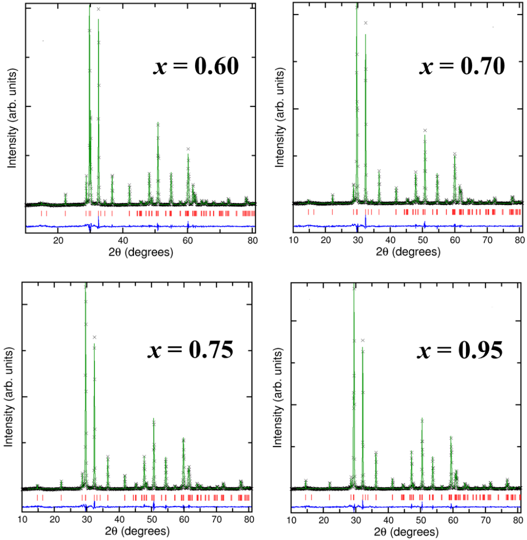

All samples are single phase

"Evolution of the local structure within chromophoric Mn-O_5 trigonal bipyramids in $YMn_{1-x}In_xO_3$ with composition," S. Mukherjee, H. Ganegoda, A. Kumar, S. Pal, C.U. Segre, and D.D. Sarma, *Inorg. Chem.* **57**, 9012–9019 (2018).

$YMn_{1-x}In_xO_3$ refinements

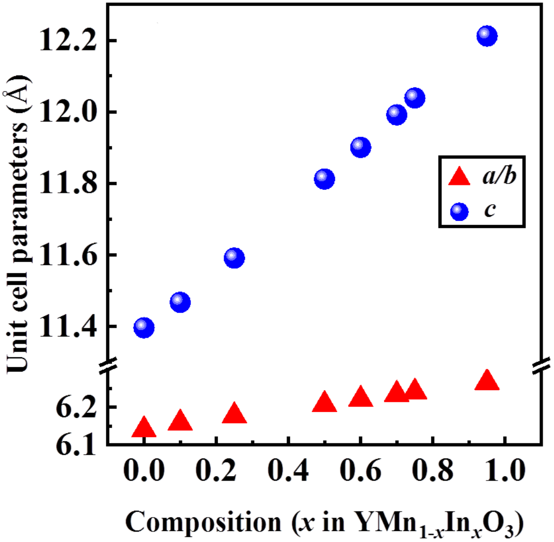

All samples are single phase

Lattice parameters vary linearly according to Vegard's law

"Evolution of the local structure within chromophoric Mn-O_5 trigonal bipyramids in $YMn_{1-x}In_xO_3$ with composition," S. Mukherjee, H. Ganegoda, A. Kumar, S. Pal, C.U. Segre, and D.D. Sarma, *Inorg. Chem.* **57**, 9012–9019 (2018).

$YMn_{1-x}In_xO_3$ refinements

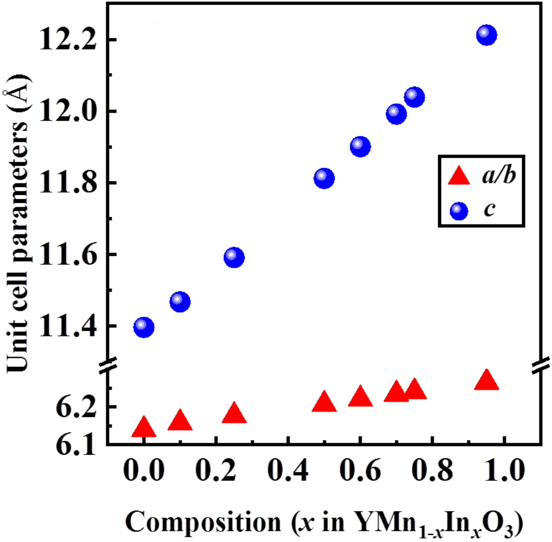

All samples are single phase

Lattice parameters vary linearly according to Vegard's law

How do the local environments of the manganese and indium vary?

"Evolution of the local structure within chromophoric Mn-O_5 trigonal bipyramids in $YMn_{1-x}In_xO_3$ with composition," S. Mukherjee, H. Ganegoda, A. Kumar, S. Pal, C.U. Segre, and D.D. Sarma, *Inorg. Chem.* **57**, 9012–9019 (2018).

$YMn_{1-x}In_xO_3$ refinements

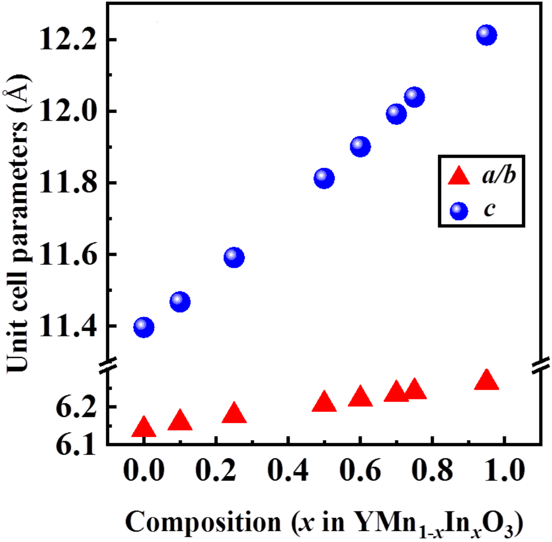

All samples are single phase

Lattice parameters vary linearly according to Vegard's law

How do the local environments of the manganese and indium vary?

Hypothesis: Smooth variation in bond distances & near neighbors

"Evolution of the local structure within chromophoric Mn-O_5 trigonal bipyramids in $YMn_{1-x}In_xO_3$ with composition," S. Mukherjee, H. Ganegoda, A. Kumar, S. Pal, C.U. Segre, and D.D. Sarma, *Inorg. Chem.* **57**, 9012–9019 (2018).

$YMn_{1-x}In_xO_3$ x-ray absorption spectroscopy

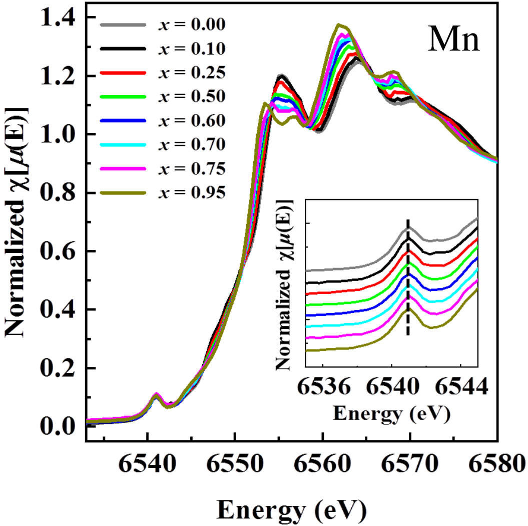

"Evolution of the local structure within chromophoric Mn-O_5 trigonal bipyramids in $YMn_{1-x}In_xO_3$ with composition," S. Mukherjee, H. Ganegoda, A. Kumar, S. Pal, C.U. Segre, and D.D. Sarma, *Inorg. Chem.* **57**, 9012–9019 (2018).

$YMn_{1-x}In_xO_3$ x-ray absorption spectroscopy

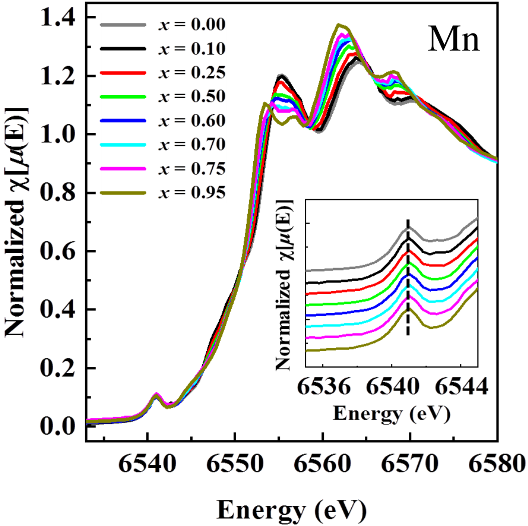

The Mn is in the +3 state throughout the series and shows a single pre-edge peak

"Evolution of the local structure within chromophoric Mn-O_5 trigonal bipyramids in $YMn_{1-x}In_xO_3$ with composition," S. Mukherjee, H. Ganegoda, A. Kumar, S. Pal, C.U. Segre, and D.D. Sarma, *Inorg. Chem.* **57**, 9012–9019 (2018).

$YMn_{1-x}In_xO_3$ x-ray absorption spectroscopy

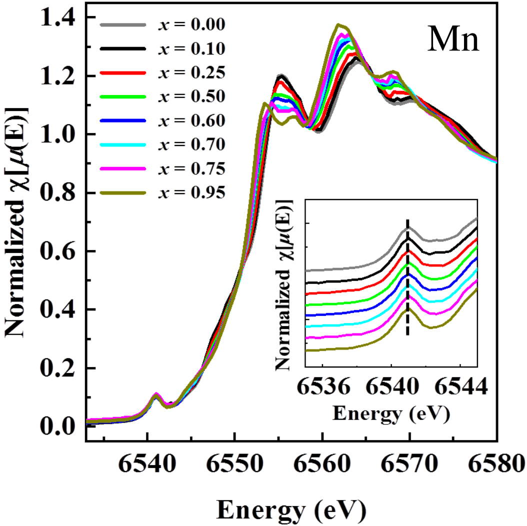

The Mn is in the +3 state throughout the series and shows a single pre-edge peak

The Mn K-edge shows distinct isosbestic points indicating that all the samples are mixtures of two different Mn local environments

"Evolution of the local structure within chromophoric Mn-O_5 trigonal bipyramids in $YMn_{1-x}In_xO_3$ with composition," S. Mukherjee, H. Ganegoda, A. Kumar, S. Pal, C.U. Segre, and D.D. Sarma, *Inorg. Chem.* **57**, 9012–9019 (2018).

$YMn_{1-x}In_xO_3$ x-ray absorption spectroscopy

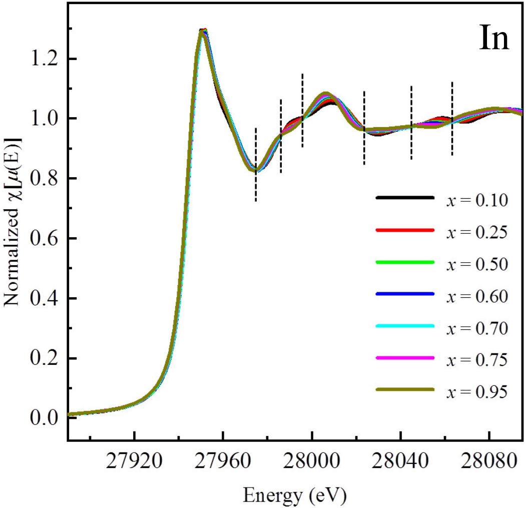

The Mn is in the +3 state throughout the series and shows a single pre-edge peak

The Mn K-edge shows distinct isosbestic points indicating that all the samples are mixtures of two different Mn local environments

Similar isosbestic points appear at the In K-edge

"Evolution of the local structure within chromophoric Mn-O_5 trigonal bipyramids in $YMn_{1-x}In_xO_3$ with composition," S. Mukherjee, H. Ganegoda, A. Kumar, S. Pal, C.U. Segre, and D.D. Sarma, *Inorg. Chem.* **57**, 9012–9019 (2018).

Bimodal Mn local environment fits XANES

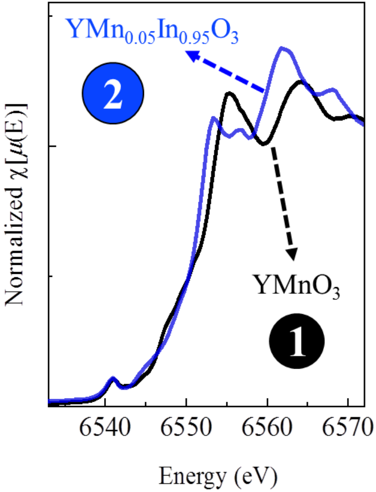

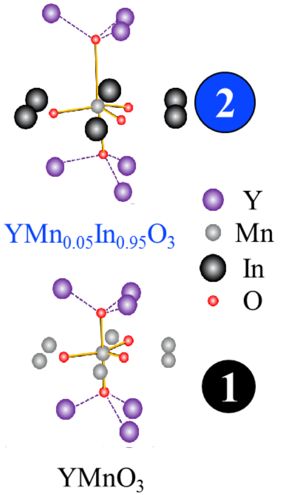

Fit endpoints with two different Mn local environments

"Evolution of the local structure within chromophoric Mn-O_5 trigonal bipyramids in $YMn_{1-x}In_xO_3$ with composition," S. Mukherjee, H. Ganegoda, A. Kumar, S. Pal, C.U. Segre, and D.D. Sarma, *Inorg. Chem.* **57**, 9012–9019 (2018).

Bimodal Mn local environment fits XANES

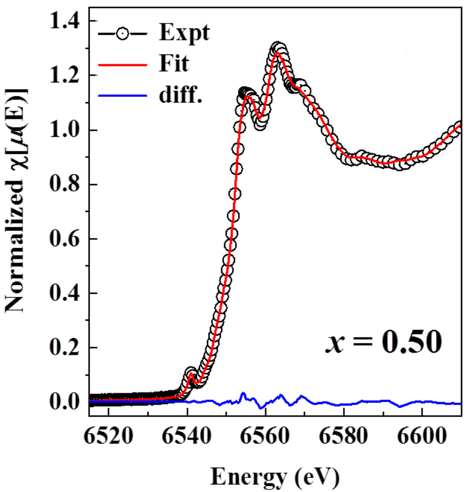

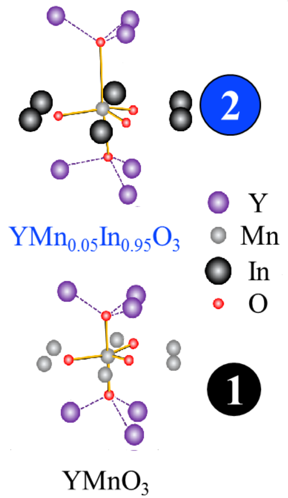

Fit endpoints with two different Mn local environments then fit all spectra with a linear combination of the two

"Evolution of the local structure within chromophoric Mn-O_5 trigonal bipyramids in $YMn_{1-x}In_xO_3$ with composition," S. Mukherjee, H. Ganegoda, A. Kumar, S. Pal, C.U. Segre, and D.D. Sarma, *Inorg. Chem.* **57**, 9012–9019 (2018).

Detailed modeling of endpoint compositions

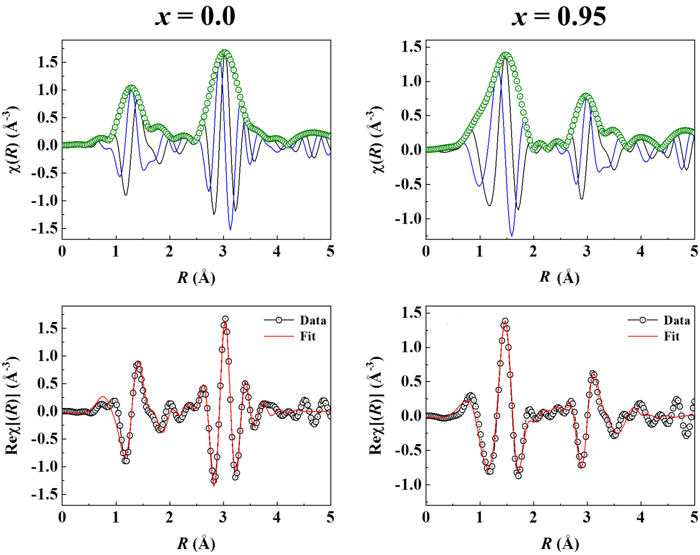

"Evolution of the local structure within chromophoric Mn-O$_5$ trigonal bipyramids in YMn$_{1-x}$In$_x$O$_3$ with composition," S. Mukherjee, H. Ganegoda, A. Kumar, S. Pal, C.U. Segre, and D.D. Sarma, *Inorg. Chem.* **57**, 9012–9019 (2018).

Endpoint EXAFS fits describe all samples

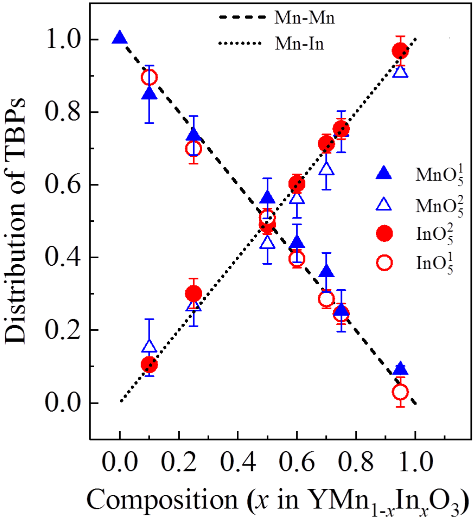

The EXAFS of both Mn and In edges of all samples can be fit by a linear combination of the two endpoint models with only one variable parameter

"Evolution of the local structure within chromophoric Mn-O_5 trigonal bipyramids in $YMn_{1-x}In_xO_3$ with composition," S. Mukherjee, H. Ganegoda, A. Kumar, S. Pal, C.U. Segre, and D.D. Sarma, *Inorg. Chem.* **57**, 9012–9019 (2018).

Endpoint EXAFS fits describe all samples

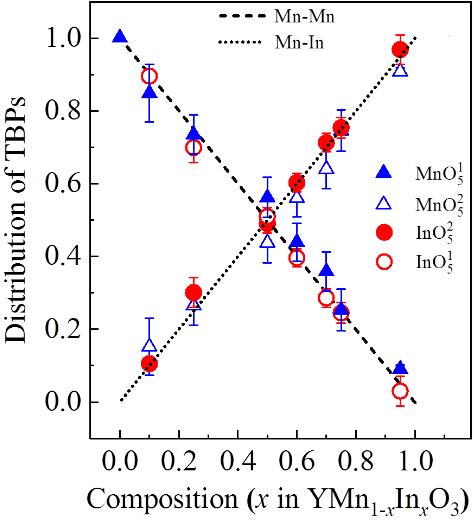

The EXAFS of both Mn and In edges of all samples can be fit by a linear combination of the two endpoint models with only one variable parameter

Conclude that Mn and In have segregated into Mn-rich and In-rich domains which must be nanometer sized

"Evolution of the local structure within chromophoric Mn-O_5 trigonal bipyramids in $YMn_{1-x}In_xO_3$ with composition," S. Mukherjee, H. Ganegoda, A. Kumar, S. Pal, C.U. Segre, and D.D. Sarma, *Inorg. Chem.* **57**, 9012–9019 (2018).

Endpoint EXAFS fits describe all samples

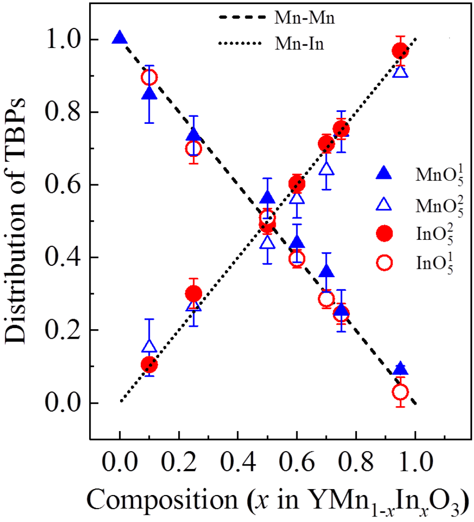

The EXAFS of both Mn and In edges of all samples can be fit by a linear combination of the two endpoint models with only one variable parameter

Conclude that Mn and In have segregated into Mn-rich and In-rich domains which must be nanometer sized

This must mean that the color is due to dilute Mn in the In-rich environment and that the color must be invariant across the series

"Evolution of the local structure within chromophoric Mn-O_5 trigonal bipyramids in $YMn_{1-x}In_xO_3$ with composition," S. Mukherjee, H. Ganegoda, A. Kumar, S. Pal, C.U. Segre, and D.D. Sarma, *Inorg. Chem.* **57**, 9012–9019 (2018).

$YMn_{1-x}In_xO_3$ optical properties

With the XAS results in mind, let's revisit the optical absorption results

"Evolution of the local structure within chromophoric Mn-O_5 trigonal bipyramids in $YMn_{1-x}In_xO_3$ with composition," S. Mukherjee, H. Ganegoda, A. Kumar, S. Pal, C.U. Segre, and D.D. Sarma, *Inorg. Chem.* **57**, 9012–9019 (2018).

$YMn_{1-x}In_xO_3$ optical properties

With the XAS results in mind, let's revisit the optical absorption results

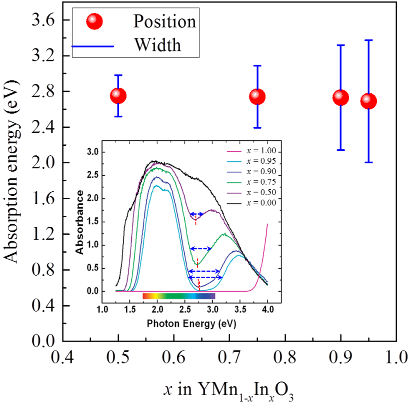

"Evolution of the local structure within chromophoric Mn-O_5 trigonal bipyramids in $YMn_{1-x}In_xO_3$ with composition," S. Mukherjee, H. Ganegoda, A. Kumar, S. Pal, C.U. Segre, and D.D. Sarma, *Inorg. Chem.* **57**, 9012–9019 (2018).

$YMn_{1-x}In_xO_3$ optical properties

With the XAS results in mind, let's revisit the optical absorption results

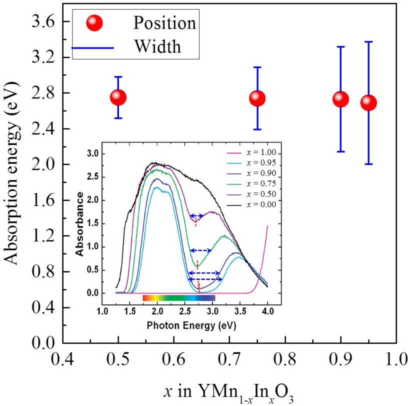

The centroid of the absorption band remains constant and the concentration only affects the width of the band

"Evolution of the local structure within chromophoric Mn-O_5 trigonal bipyramids in $YMn_{1-x}In_xO_3$ with composition," S. Mukherjee, H. Ganegoda, A. Kumar, S. Pal, C.U. Segre, and D.D. Sarma, *Inorg. Chem.* **57**, 9012–9019 (2018).

$YMn_{1-x}In_xO_3$ optical properties

With the XAS results in mind, let's revisit the optical absorption results

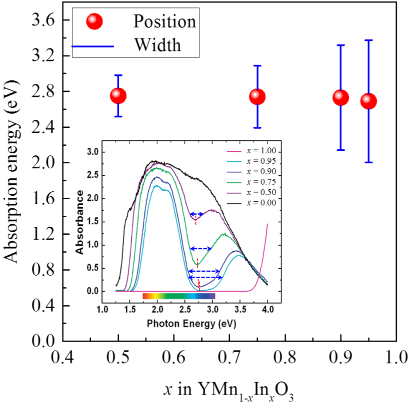

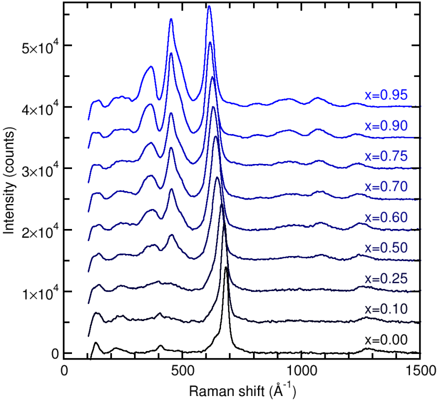

The centroid of the absorption band remains constant and the concentration only affects the width of the band

"Evolution of the local structure within chromophoric Mn-O_5 trigonal bipyramids in $YMn_{1-x}In_xO_3$ with composition," S. Mukherjee, H. Ganegoda, A. Kumar, S. Pal, C.U. Segre, and D.D. Sarma, *Inorg. Chem.* **57**, 9012–9019 (2018).

$YMn_{1-x}In_xO_3$ optical properties

With the XAS results in mind, let's revisit the optical absorption results

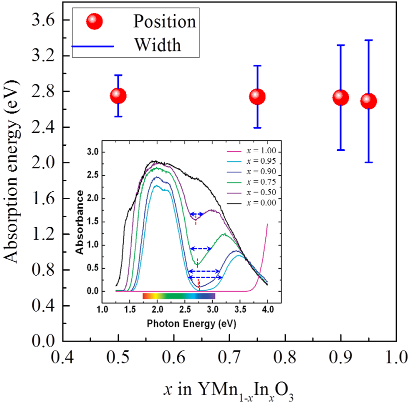

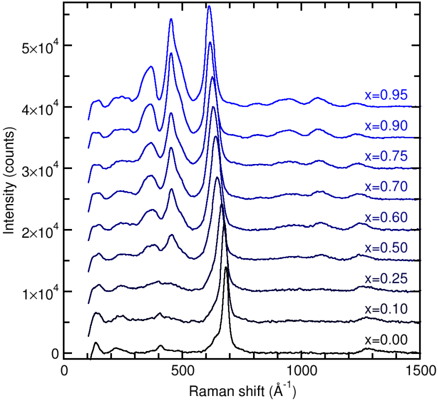

The centroid of the absorption band remains constant and the concentration only affects the width of the band

The Raman scattering data are also consistent with the XAS results

"Evolution of the local structure within chromophoric Mn-O_5 trigonal bipyramids in $YMn_{1-x}In_xO_3$ with composition," S. Mukherjee, H. Ganegoda, A. Kumar, S. Pal, C.U. Segre, and D.D. Sarma, *Inorg. Chem.* **57**, 9012–9019 (2018).

Purple $YMn_{1-x}Ga_xO_3$ solid solution

$YGaO_3$ has same hexagonal structure

Purple $YMn_{1-x}Ga_xO_3$ solid solution

$YGaO_3$ has same hexagonal structure

Doping with Mn gives brilliant purple colors

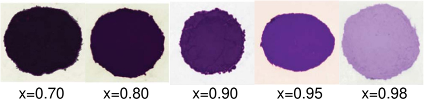

Purple $YMn_{1-x}Ga_xO_3$ solid solution

$YGaO_3$ has same hexagonal structure

Doping with Mn gives brilliant purple colors

Is Mn in a bimodal local environment?

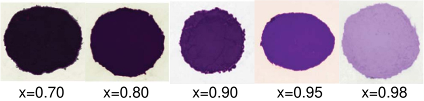

Purple $YMn_{1-x}Ga_xO_3$ solid solution

$YGaO_3$ has same hexagonal structure

Doping with Mn gives brilliant purple colors

Is Mn in a bimodal local environment?

$YMn_{1-x}Ga_xO_3$ is more challenging, requiring careful control of temperature and time to avoid garnet impurity phase

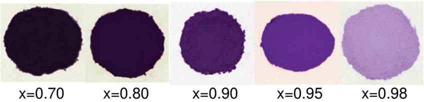

Purple $YMn_{1-x}Ga_xO_3$ solid solution

$YGaO_3$ has same hexagonal structure

Doping with Mn gives brilliant purple colors

Is Mn in a bimodal local environment?

$YMn_{1-x}Ga_xO_3$ is more challenging, requiring careful control of temperature and time to avoid garnet impurity phase


x=0.70


x=0.80


x=0.90


x=0.95


x=0.98

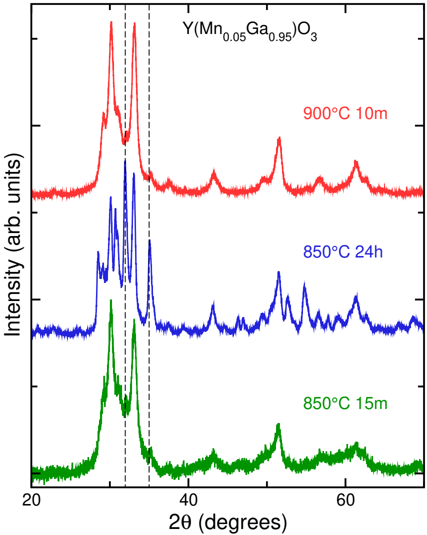

$YMn_{1-x}Ga_xO_3$ diffraction data

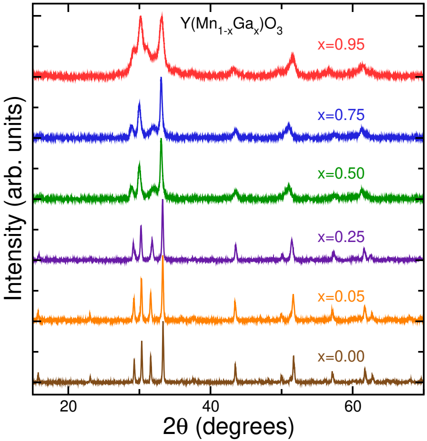

$YMn_{1-x}Ga_xO_3$ diffraction data

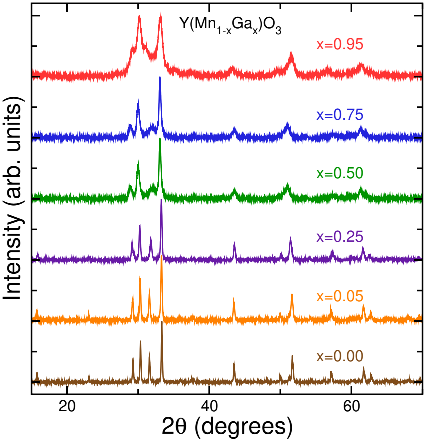

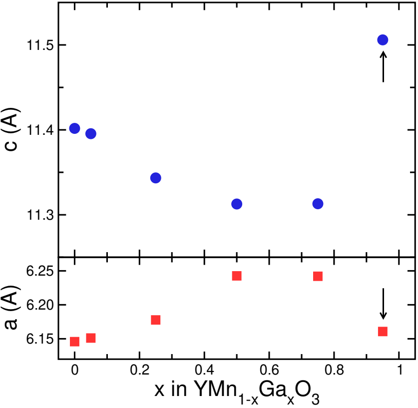

$YMn_{1-x}Ga_xO_3$ XANES

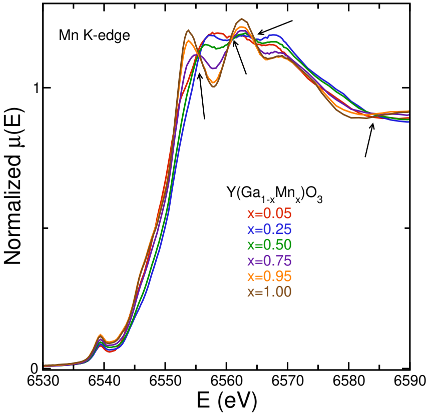

$YMn_{1-x}Ga_xO_3$ XANES

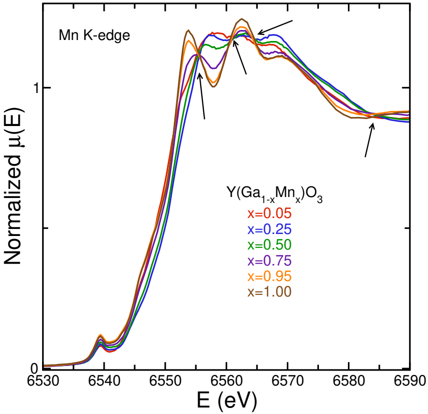

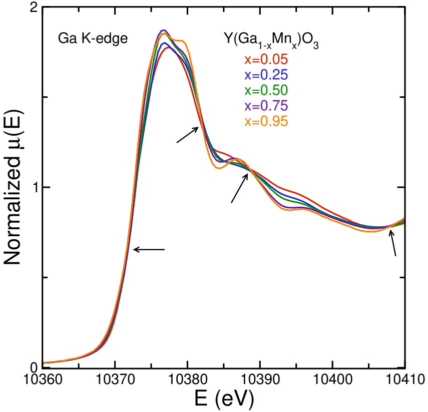

$YMn_{1-x}Ga_xO_3$ EXAFS

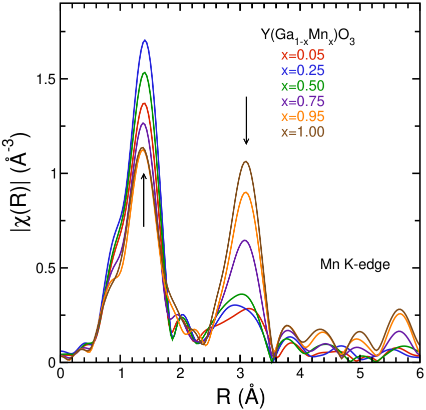

$YMn_{1-x}Ga_xO_3$ EXAFS

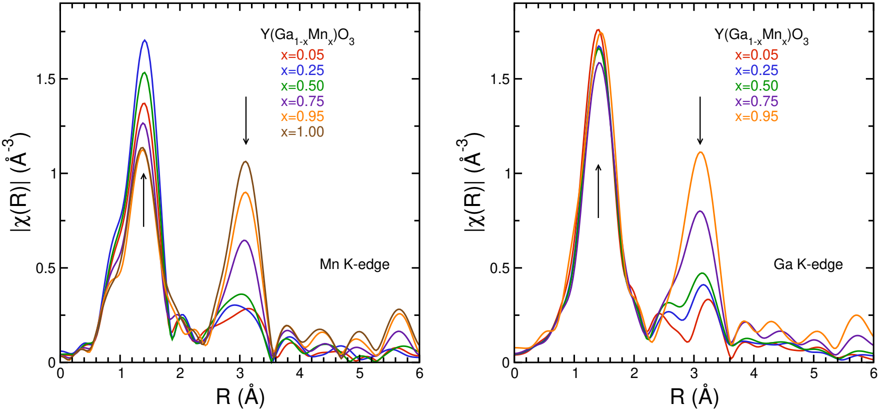

Where do we go from here?

$YMn_{1-x}Ga_xO_3$ needs additional work to obtain good crystalline samples across the composition range

Where do we go from here?

$YMn_{1-x}Ga_xO_3$ needs additional work to obtain good crystalline samples across the composition range

Bimodal environments seem to be a general property of the two systems studied so far

Where do we go from here?

$YMn_{1-x}Ga_xO_3$ needs additional work to obtain good crystalline samples across the composition range

Bimodal environments seem to be a general property of the two systems studied so far

Will this bimodal environment be present in all systems based on this hexagonal structure? In other chromophore systems?